Master Thesis

The effect of the North-East Greenland Ice Stream (NEGIS) on the Greenland ice sheet in changing climates

(気候変動下におけるグリーンランド氷床での北東グリーンランド氷流のもたらす影響)

Shoko Otsu

MS Course for Pioneer Research

Graduate School of Environmental Science

Division of Environmental Science Development

Hokkaido University

March 2007

Contents

Abstract (English) 3
Abstract (Japanese) 5

1. Introduction 7
1.1 General background ・・・・・・・・・・・・・・・・・・・・・・・・・・・・・7
1.2 Review of previous modeling research ・・・・・・・・・・・・・・・・・10
1.3 Specific research problems 12
1.3.1 The North-east Greenland ice stream ・・・・・・・・・12
1.3.2 Surface meltwater influence ・・・・・・・・・・・・・・17
1.4 Goals of this study ・・・・・・・・・・・・・・・・・・・・・・・・・・19

2. Dynamics of ice sheets 20
2.1 Balance equations ・・・・・・・・・・・・・・・・・・・・・・・・・・・20
2.2 Mechanism of ice flow ・・・・・・・・・・・・・・・・・・・・・・・・22
2.3 Temperature equation ・・・・・・・・・・・・・・・・・・・・・・・・25
2.4 Boundary conditions ・・・・・・・・・・・・・・・・・・・・・・・・・25
2.5 The evolution of ice thickness ・・・・・・・・・・・・・・・・・・・26

3. Model description 29
3.1 SICOPOLIS ・・・・・・・・・・・・・・・・・・・・・・・・・・・・・・29
3.2 General set-ups 31
3.2.1 Basal sliding condition ・・・・・・・・・・・・・・・・・31
3.2.2 Paleoclimatic forcing ・・・・・・・・・・・・・・・・・33
3.2.3 Future climatic forcing: WRE scenarios ・・・・・・・35
3.2.4 Surface meltwater ・・・・・・・・・・・・・・・・・・・37
3.2.5 Other physical parameters ・・・・・・・・・・・・・・39

4. Paleoclimatic simulations 40
4.1 Set-up of GRL20: 20 km grid ・・・・・・・・・・・・・・・・・・・・40
4.1.1 Results and discussion of the reference simulation without the NEGIS (GRL20_REF) ・・・・・・・・・・・・・・・・・・・42
4.1.2 Results and discussion of simulations with varied basal sliding coefficient (GRL20_ BSC) ・・・・・・・・・・・・・・・・・42

4.1.3 Results and discussion of simulations with varied surface meltwater coefficient (GRL20_SMW) ・・・・・・・・・・・・・・・ 47
4.1.4 Conclusion of GRL20 and motivation for next simulations ・・ 51
4.2 Set-up of GRL10: 10 km grid ・・・・・・・・・・・・・・・・・・・・・ 51
4.2.1 Result and discussion of the reference simulation without the NEGIS (GRL10_REF) ・・・・・・・・・・・・・・・・・・・・ 52
4.2.2 Results and discussion of simulations with varied basal sliding coefficient for non-linear basal sliding (GRL10_ BSC) ・・・・・・・ 52
4.2.3 Results and discussion of simulations with varied basal sliding coefficient for linear basal sliding (GRL10_ BSCL) ・・・・・・・・ 59
4.2.4 Conclusion of GRL10 ・・・・・・・・・・・・・・・・・・・・ 61

5. Future simulations 63
5.1 Set-up of WRE10 ・・・・・・・・・・・・・・・・・・・・・・・・・ 63
5.2 Results and discussion of the reference simulation without surface meltwater effect and without NEGIS (WRE10_WRE_REF) ・・・・・・・・ 63
5.3 Results and discussion of simulations with enhanced basal sliding and surface meltwater effect for the NEGIS (WRE10_WRE_SMW) ・・・・・・ 64
5.3' Mini surge ・・・・・・・・・・・・・・・・・・・・・・・・・・・ 68
5.4 Results and discussion of simulations with enhanced basal sliding for the NEGIS and surface meltwater effect for the entire ice sheet (WRE10_WRE_SMWALL) ・・・・・・・・・・・・・・・・・・・・・・ 70
5.5 Conclusion of WRE10 ・・・・・・・・・・・・・・・・・・・・・・・ 72

6. Summary 73

7. Acknowledgments 74

8. References 75

Abstract

The North-East Greenland Ice Stream (NEGIS) was discovered as a large fast-flow feature in north-east Greenland by synthetic aperture radar (SAR) imaginary of the ERS-1 satellite. In this study, the NEGIS is implemented in the ice-sheet model SICOPOLIS (Simulation Code for POLythermal Ice Sheets), which simulates the large-scale dynamics and thermodynamics of an ice sheet three-dimensionally and over time.

In the first part of my study, paleoclimatic simulations are carried out. We simulate the evolution of the ice sheet on a 20-km grid for the period from 250 ka BP until today. Spin-up simulations are from 422 ka BP until 250 ka BP, and the time step for all model components is 5 a. It is driven by a climatology reconstructed from a combination of present-day observations and GCM results for the past. In the 20-km resolution runs, we employ two different types of simulations, one is variation of the basal sliding coefficient in the Weertman sliding law for the NEGIS area, and the other is consideration of the effect of surface melt-water to basal sliding at NEGIS. We assume that the NEGIS area is characterized by enhanced basal sliding compared to the “normal”, slowly-flowing areas of the ice sheet, and optimize the basal sliding law in the NEGIS area by minimizing the misfit between simulated and observed surface elevations and velocities. Tuning the basal sliding coefficient shows a very clear effect on the NEGIS, and by comparison with velocity data, provides a reasonable value of the coefficient. On the other hand, the surface melt-water affects only the ice margin, and therefore cannot explain the onset of the NEGIS as far upstream as observed.

In the second step, 10-km resolution simulations are carried out with a modified domain map based on Fahnestock et al. (1993) in order to have a more detailed representation of the NEGIS. The model time is from 127 ka BP until today without spin-up simulations, and the time step for all model components is 1 a. Like for the 20-km simulations, fast sliding in the NEGIS area is implemented by an enhanced basal sliding coefficient. By comparison with date for the velocity and the ice thickness, it is concluded that an enhancement by a factor three gives the best results.

Then, the role of the NEGIS for the possible decay of the Greenland ice sheet in future warming climates is investigated. Recent observations of accelerated ice flow in Greenland indicate that surface melt-water percolating to the base may play a crucial role in provoking a fast reaction of ice-sheet flow on increased surface temperatures. By employing a simple, plausible parameterization of this process for the NEGIS area, we

simulate the evolution of the ice sheet over the next centuries in response to standard greenhouse-gas-emission scenarios, and look into the question whether an accelerating NEGIS can affect the stability of the ice sheet as a whole. For future warming scenarios, the effect of the NEGIS (the best basal sliding coefficient) and the variation of the surface meltwater coefficient are investigated. Moreover, we model the surface meltwater effect on the entire ice sheet with the same settings of the basal sliding coefficient of the NEGIS and the climate conditions. From the result of the runs, we find that the surface meltwater effect (when limited to the NEGIS) on the total volume of ice sheet is quite small, while the variation of global warming scenarios affect the ice volume strongly. However, the surface meltwater effect is pronounced when applied to the entire ice sheet and very high values for the surface meltwater coefficient are assumed. It is obvious that ice melts strongly in large areas especially in southern Greenland where temperatures are generally higher.

要旨

人工衛星 ERS-1 の合成開口レーダー(SAR)によって大規模な速い氷の流れが見出され、北東グリーンランド氷流(NEGIS)がグリーンランドの北東部に発見された。本研究では3次元動力学/熱力学的氷床モデル SICOPOLIS (Simulation Code for POLythermal Icœ Sheets)を用いてこの NEGIS がグリーンランド氷床の変動に与える影響を明らかにする。

研究の第一段階として 25 万年前から現在の氷床変動の数値実験を行う。42 万 2 千年前から 25 万年前までの計算結果を初期条件として、空間・時間分解能はそれぞれ 20km と 5 年に設定する。モデル中の気候条件は、観測値で得られた現在の気候条件と GCM の結果から得られた過去の気候条件を組み合わせて再現された指標に基づいて計算する。20km グリッドの実験では、NEGIS の領域で Weertman 底面滑り則の底面滑り係数を変化させる実験と、NEGIS での底面滑りに与える表面融解水の影響を考慮する実験の二種類を実行する。氷床の大部分を占める"通常"のゆっくりとした氷の流れに対し、NEGIS の領域では底面滑りを変化させる事によってその領域に速い氷流を表現する。氷床表面高度と表面流動速度のそれぞれにおいて、数値実験の結果と観測値を比較し、その差が最小になる底面滑り則の係数値を最適な値とみなす。底面滑り係数の変動は NEGIS に顕著な影響を示し、氷床表面速度の観測結果との比較により妥当な係数の値を得ることができた。一方、NEGIS の領域での表面融解水の底面滑りに与えうる影響は、簡単で妥当なパラメーター(表面融解水係数)を用いて導入する。その結果、表面融解水の影響は氷床末端にとどまり、それゆえ実際に観測されているようなはるか内陸の上流部にまで及ぶ NEGIS の特徴を表面融解水の影響のみから説明できないことが明らかになった。

研究の第二段階として、改良された NEGIS の領域を用いた 10km のグリッドの数値実験を行う。これは Fahnestock ら(1993)によるグリーンランド氷床表面の衛星観測結果を基にしており、NEGIS の存在領域をより詳しく表現するためのものである。計算する期間は 12 万 7 千年から現在までであり、初期条件には予め計算された氷床の情報を用い、時間分解能は 1 年に設定する。20km グリッドの数値実験と同様、NEGIS の速い氷流は底面滑り係数を変化させる事によって表される。実験の結果、氷床表面速度と表面高度の観測結果との比較によって、通常の滑り係数の 3 倍の値が最適であると結論づけられた。

次に、NEGIS がグリーンランド氷床の変動において、将来の温暖化気候下ではどのような影響を与えるかを予測する実験を行う。今日のグリーンランドでの氷流加速の観測結果は、氷床表面気温上昇によって生じた融解水が氷床底面まで浸透して流動を促進することで、気候の変動が短い応答時間で氷床の流動に影響を与え得ることを示唆している。そこで表面融解水係数を用いて標準的な温暖化ガス放出シナリオ下で数世紀に渡って氷床成長を計算し、その結果を従来のモデル結果と比較する事によって、温暖化によって表面

融解が増加したときに NEGIS が氷床全体の安定性に影響を及ぼし得るかどうかについて調べる。この実験では NEGIS の影響（最適な底面滑り係数）に加えて表面融解水係数を変化させた計算を行う。さらに同じ条件で、表面融解水の影響を氷床全体に与えた場合についても数値実験を行う。計算の結果から、表面融解水の影響を NEGIS に制限した場合に表面融解水の氷床の全氷体積への影響はかなり小さく、一方で温暖化シナリオを変えることによる氷体積への影響は非常に大きいことがわかった。しかしながら、表面融解水の影響を氷床全体に適用し、しかもかなり大きな値を見積もった場合には氷体積への影響は顕著であり、概して気温の高いグリーンランド南部での氷床の後退が特に著しいこと明らかになった。

1. Introduction

1.1 General background

It is a well-documented fact that the earth has been getting warmer recently, and the effect can not be neglected any more. One of the most sensitive elements for warming climates in nature is snow and ice. The major part of snow and ice masses exists as glaciers and ice sheets, especially the ice sheets in Greenland and Antarctica. The Greenland ice sheet is the second-largest ice mass on the present-day earth. The amount of its ice volume is 2.9×10^6 km^3, and the ice-covered area is 1.7×10^6 km^2, which equals 7.5 m of sea-level equivalent (Bamber et al., 2001b). It is estimated that the mass loss of the ice sheet is composed of approximately 50% melting and 50% calving (the decay from the margins) (Ohmura 2004, Huybrechts, P. et al., 1991), that is, plenty of melting is caused by global warming. The effect of the warming must be significant, and will lead to a large decay of the ice sheet.

As a remarkable topic in recent scientific research on global warming, the melt water from glaciers and ice sheets is provoking the sea-level rise. In the third assessment report of IPCC (Intergovernmental Panel on Climate Change), Church et al. (2001) note that estimates from modeling studies have led to contributions of between 0.0 to 0.1 mm / a (corresponding to a negative mass balance of －50 ~ －90 km^3 / a) during the 20th century from the Greenland ice sheet, and another value between 0.15 to 0.25 mm / a was reported by Ohmura (2004), who compiled the reliable data from various places in the world. It is also estimated in IPCC that the sea level changes from 1990 to 2100 with the IS92a emission scenario (a middle of the range scenario in which population rises to 11.3 billion by 2100, economic growth averages 2.3 % / a between 1990 and 2100 and a mix of conventional and renewable energy sources are used) (Leggett et al., 1992) due to the Greenland ice sheet is －0.02 ~ 0.09 m. New results from satellite-based (GRACE) gravity measurements indicate that the total mass loss of the ice sheet is －239 ± 23 km^3 / a during the period from April 2002 to November 2005 (Chen et al. 2007). There is still uncertainty in the assessment; however, ice is surely melting due to the recent global warming.

Ice streams are notable features, which show significantly faster ice flow than the surrounding ice because of their basal topographic characteristics. Two major ice streams of the Greenland ice sheet are Jakobshavn Ice Stream (JIS) located in central west Greenland, and the North-East Greenland Ice Stream (NEGIS). It is researched

that each of them drains ≈ 10 % of the coastward mass flux of the Greenland ice sheet. The flow speed in JIS has doubled since 1995, and the acceleration led to maximum values of 13 km / a in 2002 ~ 2003 (Joughin et al. 2004). Although there is no direct connection between ice melting and ice streams, ice streams can lead to a decay of ice sheets via fast flow. Some previous researches (e.g. Iken et al., 1983) suggest that surface meltwater accelerates the ice streams.

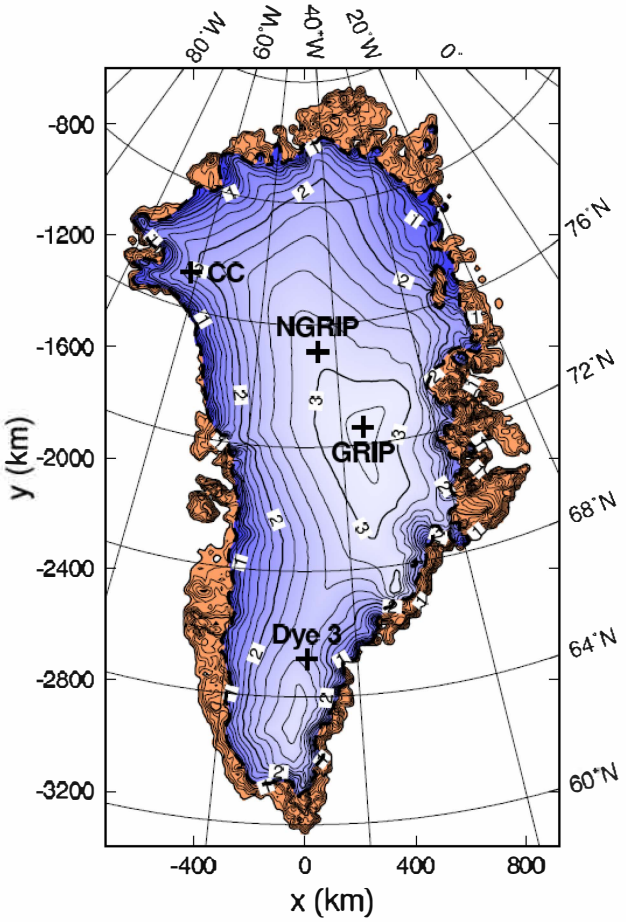

Figure 1. Surface topography of the Greenland ice sheet by Bamber et al. (2001b,c) Contour spacing is 200 m, labels are in km a.s.l., and the ice-core location GRIP, NGRIP, Camp Century, Dye 3 are indicated. Brown areas mark ice-free land.

1.2 Review of previous modeling research

The topography of Greenland is well researched (Bamber et al. 2001b, c) (Figure 1) and the surface velocity is measured around the 2000 meter elevation contour (Thomas et al. 1998). PARCA (Program for Regional Climate Assessment) also provides a data set maintained by NASA which aims at measuring and understanding the mass balance of the Greenland ice sheet. Moreover, four deep ice cores, Greenland ice core project (GRIP), NorthGRIP (NGRIP), Camp Century (CC) and Dye 3, were obtained which provide information of the surface climate history until 250,000 years into the past.

Several studies on the Greenland ice sheet have been carried out with three dimensional thermomechanical ice sheet models (Letreguilly et al. 1991, Calov and Hutter 1996, Ritz et al. 1997, Greve et al.1998, 1999, van de Wal 1991, Marshall and Cuffey 2000, Huybrechts 2002, Tarasov and Peltier 2003). Greve and Hutter (1995) found the significance of the input values of the geothermal heat flux. Subsequently, the model SICOPOLIS invented by Greve (1997a) was applied to the Greenland ice sheet (Greve 1997b), and was run with several types of parameters in two different steady climates, as well as three transient scenarios, such as sinusoidal Milankovic-period forcing, paleoclimatic forcing from the GRIP core reconstruction, and future greenhouse warming forcing. He demonstrated the effect of the geothermal heat flux distribution on the ice sheets (2005a) more precisely, which was based on the global heat-flow representation by Pollack et al. (1993), and was modified by using temperature data of the deep ice cores (Figure 2).

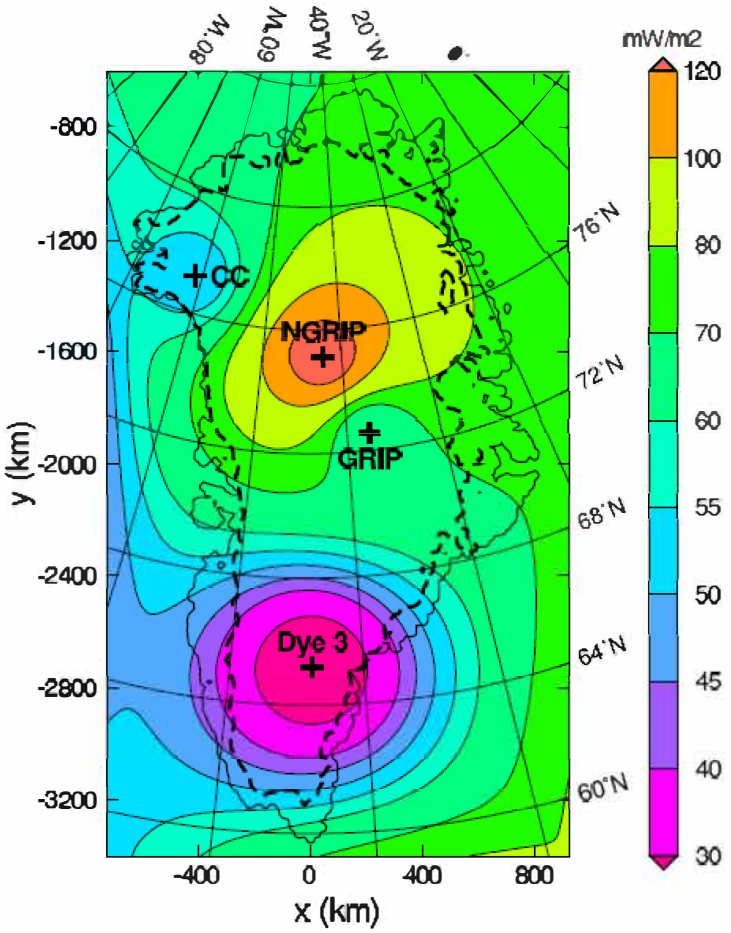

Figure 2. Distribution of the geothermal heat flux based on Pollack et al. (1993) modified with the values of GRIP, NGRIP, Camp Century and Dye 3 by Greve (2005a). The heavy dashed line indicates the present-day ice margin.

1.3 Specific research problems

1.3.1 The North-east Greenland ice stream

The large ice flow feature in northeast Greenland was discovered first by Fahnestock et al. (1993) (Figure 3(a), 3(b)). It was found by means of C-band synthetic aperture radar (SAR) imagery from the European Space Agency's ERS-1 satellite, and the feature was called 'North-east Greenland ice stream' (NEGIS) afterward. The satellite showed the backscatter signatures of snowpack which varies with the balance of accumulation and melt at various elevations. As well as visible band Advanced Very High Resolution Radiometer (AVHRR) imagery indicated, SAR also revealed the characteristic surface topography in northeast Greenland. This feature must be dynamically generated by enhanced ice flow. Beside it, the faint streaky character of the margins suggested that the margins were sites of shear strain, which elongates features within the region where the velocity gradient is high. The ice flow originates in the interior ice sheet, some 550 km from the coast, and flows north-northeastward. Its width is ~ 20 km initially, and becomes ~ 70 km wide 400 km from the coast. This width is maintained for 150 to 200 km, until it becomes more difficult to identify. Since the flow is located along the axis of the broad topographic basin, it is likely that the feature plays an important role in the ice dynamics of this region and is responsible for the morphology of the basin.

Fahnestock et al. (2001) have traced internal layers along a flight track flown by NASA P-3 Aircraft carrying a University of Kansas ice-penetrating radar and a NASA laser altimeter. They revealed the high melt rate and onset of rapid ice flow in the large ice stream. To evaluate the relation of internal layering and basal melting, the age-depth relation is taken which is determined by the balance between surface accumulation of snow and thinning of ice due to the horizontal gradient in flow speed. With the age-depth relations, they detected very high rates of melting on the northern flank of the summit dome (Figure 4(a), 4(b)). The high melt rates coincide with the disturbed topography associated with rapid flow that begins in this region. In addition, the disturbance of internal layering caused by basal melting was also visible in individual radar profiles. The basal melt rate indicated geothermal fluxes 15 to 30 times higher than the continental background. Although the origin of the high geothermal heat is not revealed, they measured that there was a gravity high, a locally strong magnetized area at the southern limit of rapid basal melt, and a coincident topographic edifice in the bed. From these observations, they suggested as the cause of the high melt

rate a presence of a volcanic topography such as a caldera structure. In their conclusion, they suggested that meltwater produced in the area from basal ice is responsible for the onset of rapid ice flow in the large ice stream.

Moreover, a new ice thickness grid had been generated from an extensive and accurate dataset of ice thickness measurement collected during 1990s by University of Kansas. The ice thickness grid was combined with a new digital elevation model (DEM) of the ice sheet and produced a new bed elevation dataset for the whole Greenland (Bamber et al. 2001b). Comparing this dataset with balance velocity estimates for the ice sheet reveals the pattern of ice flow controlled by the bed, and the presence of the NEGIS which is clearly associated with a distinct basal trough (Figure 5).

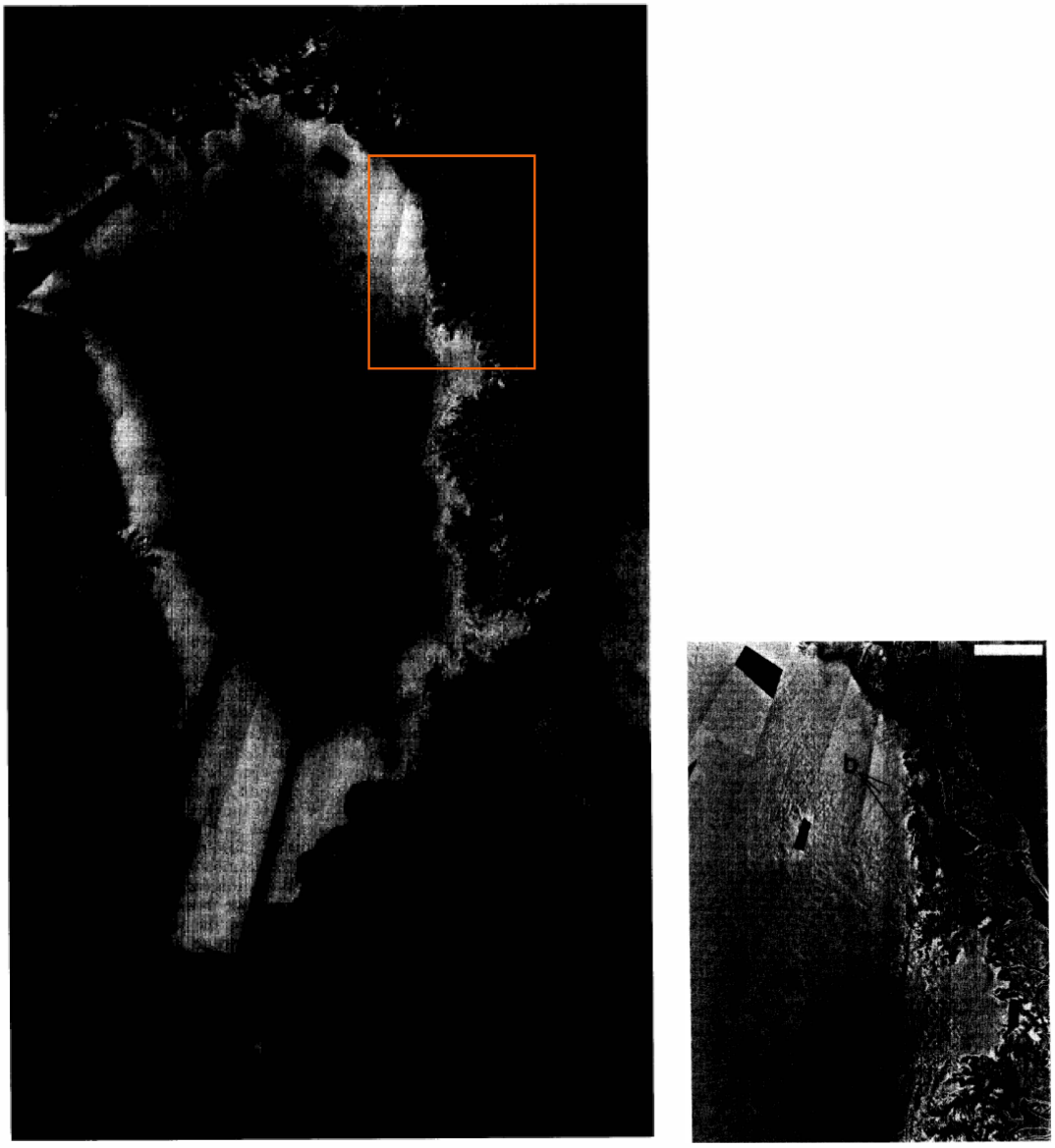

(a) (b)

Figure 3(a). Mosaic of August 1992 ERS-1 SAR imagery of the Greenland ice sheet. The mosaic is the SSM/I polar stereographic projection. A coastline has been superimposed in white.

Figure 3(b). Enlargement of Figure A1 showing a large flow feature in northeast Greenland. Scale bar is 100 km.

(Fahnestock et al., 1993)

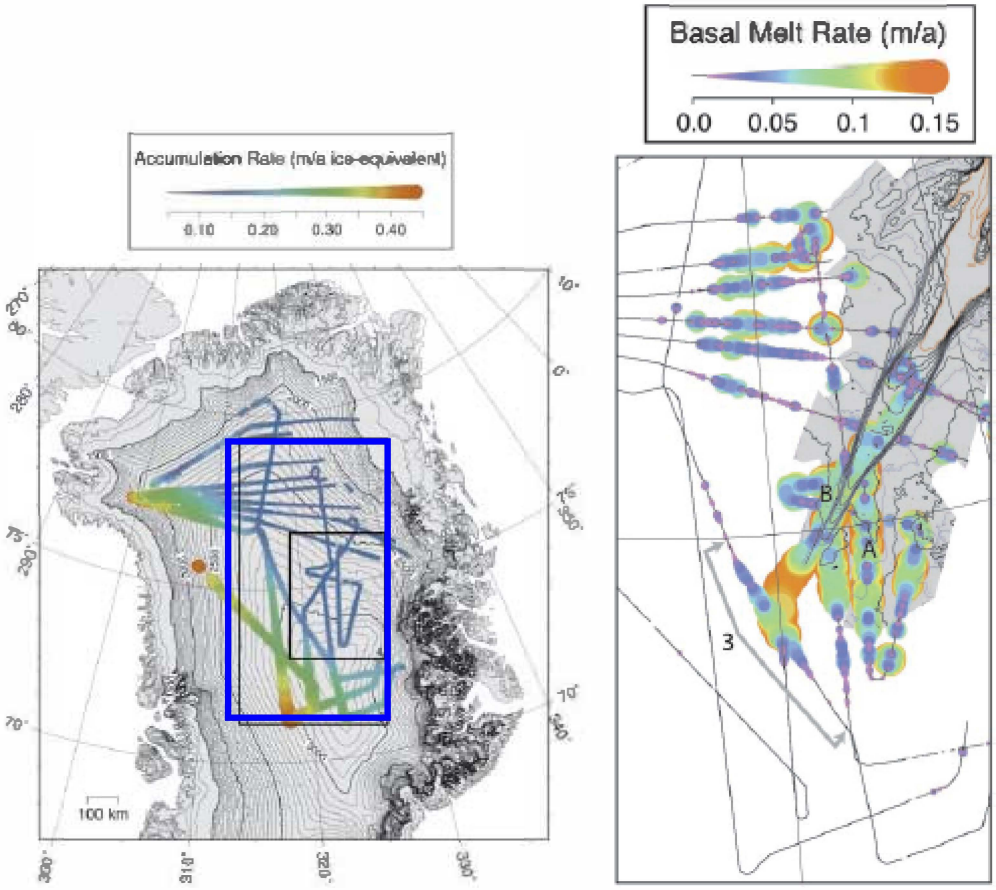

(a) (b)

Figure 4(a). Accumulation rate for the interior of the Greenland ice sheet.
Figure 4(b). Basal melt rate and rapid ice flow derived from figure 4 (a).
(Fahnestock et al. 2001)

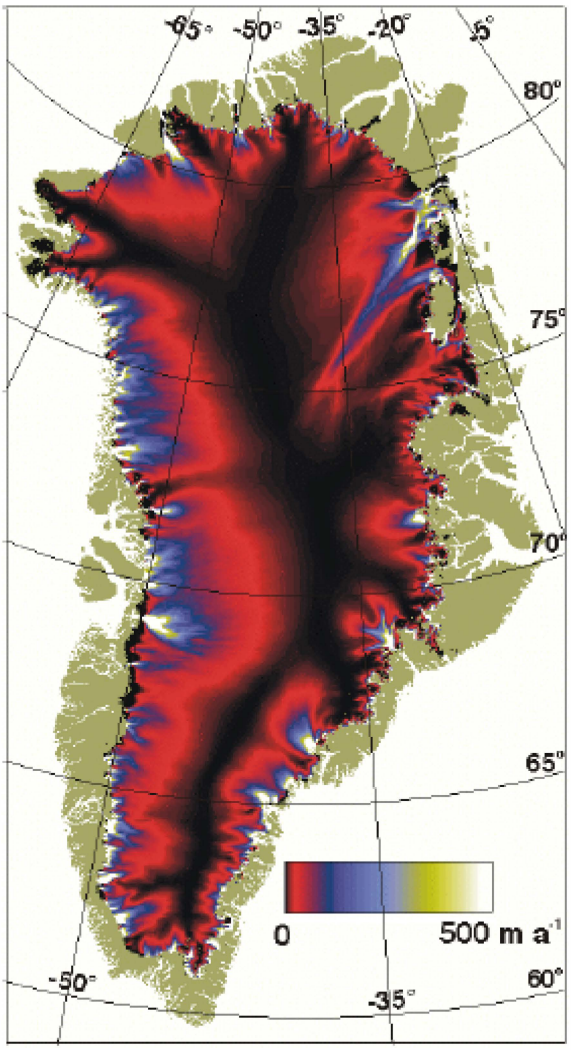

Figure 5. Contour plot of balance velocities up to 500 m / a. The contour intervals used were 10 m / a up to 50 m / a and the 50 m / a intervals above this value. (Bamber et al. 2001b)

1.3.2 Surface meltwater influence

The significant effect of surface melt-water to the basal sliding of an ice sheet was reported by Zwally et al. (2002). They observed the acceleration of ice flow during periods of summer melting in west-central Greenland at the Swiss Camp at 1175m elevation (69.57°N, 49.31°W) near the equilibrium line in June 1996. They found that the ice flow is accelerated during the period of surface melting, followed by deceleration after the melting ceases in the seasonal variation. They emphasized the acceleration mechanism. In the ablation zone, surface meltwater is collected in surface lakes or crevasses, or flows directly into moulins. The collected water penetrates quickly to the bottom through moulins, and is drained subglacially (Figure 6). When it reaches the interface between bedrock and ice, it markedly works as a basal lubricant and induces the ice acceleration.

They also presumed a mechanism which explains the acceleration by surface meltwater. The meltwater reduces the friction at the base and also lifts the ice sheet when its water pressure intensifies. This mechanism was previously reported by Iken et al. (1983) at the site of an alpine glacier. In addition to the direct effect of increased water pressure, the flow of surface water at approximately 0 ℃ to basal ice at the pressure melting point of - 1 ℃ transfers heat for additional basal melting. From these considerations, increase in surface meltwater due to climate warming might contribute to the acceleration of ice sheet flow.

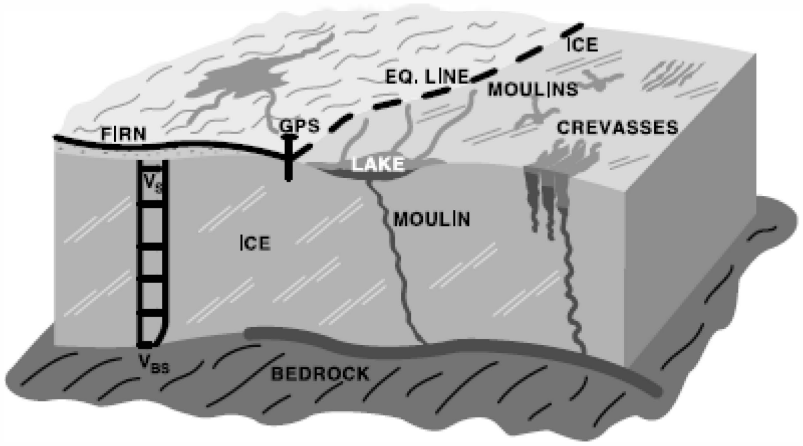

Figure 6. Schematic of glaciological features in the equilibrium and ablation zones, including surface lakes, inflow channels, crevasses, and moulins. Ice flow for basal ice at the pressure melting point is partly from basal sliding ad partly from shear deformation, which is mostly in a near-basal boundary layer. (Zwally et al., 2002)

1.4 Goals of this study

The first goal of this study is the creation of the NEGIS in paleoclimatic, 20 km resolution experiments by changing the basal sliding coefficient in the NEGIS area. It is inferred from the ice thickness deviation and comparison of surface velocity between observation and simulations. The next step is the evaluation of the influence of surface meltwater at NEGIS in the paleoclimatic runs which may cause accelerated ice flow, and therefore affects the ice volume significantly. In the 10 km resolution paleoclimatic simulations, more precise results will be obtained, and the best fit for the basal sliding coefficient will be determined. Besides, linear basal sliding, which takes place on soft sediment, will be considered at NEGIS as an alternative to non-liner sliding on hard rock.

In the future simulations, the effect of NEGIS with enhanced basal sliding coefficient and acceleration due to surface meltwater in warming climates will be studied. The surface meltwater effect is applied either at the NEGIS only, or for the entire Greenland ice sheet. The future evolution of NEGIS under several warming climate scenarios and the effect of surface meltwater on the ice sheet are interesting and important for further researches of glaciers and ice sheets in the changing climates on earth.

2. Dynamics of ice sheets

2.1 Balance equations

If we consider the properties of ice, its deformation is described as a density-preserving, non-linear (power law) viscous fluid. We first introduce the balance equations of mass, momentum and internal energy of ice, respectively,

$$\mathrm{div}\boldsymbol{v} = 0\,, \tag{2.1}$$

$$\rho\frac{d\,\boldsymbol{v}}{dt} = \mathrm{div}\boldsymbol{t} + \boldsymbol{f}\ , \tag{2.2}$$

$$\rho\frac{du}{dt} = -\mathrm{div}\,\boldsymbol{q} + \mathrm{tr}(\boldsymbol{t}\cdot\boldsymbol{D}) + \rho\boldsymbol{r}\,, \tag{2.3}$$

where $\boldsymbol{v}$ is the velocity vector, ρ the ice density, t the time , $\boldsymbol{t}$ the stress tensor, $\boldsymbol{f}$ external volume forces, u the internal energy of ice, $\boldsymbol{q}$ the heat flux, $\boldsymbol{D}$ the strain-rate tensor, and r the specific radiation power.

Equation (2.1) expresses the conservation of mass of ice. For a density-preserving (incompressible) fluid, ρ = constant, that is, the density of ice is considered to be unchanged over time. Equation (2.2) represents the momentum balance, which describes three dimensional stress balance for each point of the material. The internal energy balance is described by Equation (2.3).

The matrix of the stress tensor $\boldsymbol{t}$ is

$$\boldsymbol{t} = \begin{pmatrix} t_{xx} & t_{xy} & t_{xz} \\ t_{yx} & t_{yy} & t_{yz} \\ t_{zx} & t_{zy} & t_{zz} \end{pmatrix}. \tag{2.4}$$

Here, the three diagonal elements (t_{xx}, t_{yy}, t_{zz}) are referred to as normal stresses, and the six off-diagonal elements $(t_{xy}, t_{yx}, t_{xz}, t_{zx}, t_{yz}, t_{zy})$ are called shear stresses. The meaning of these components is illustrated in Figure 7.

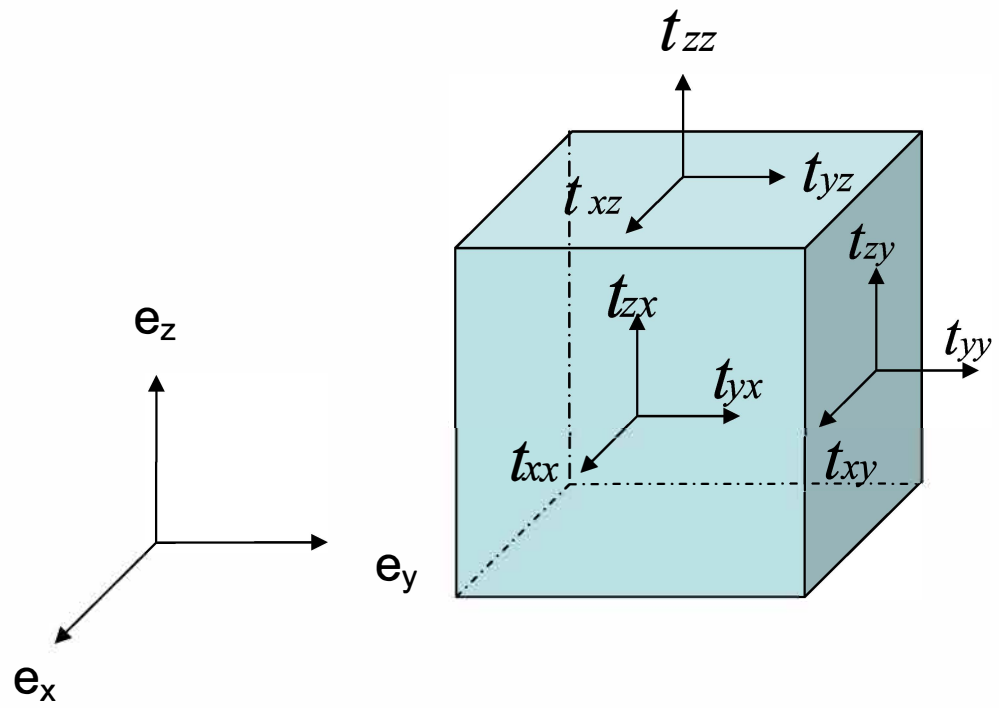

Figure 7. Stress components in a three dimensional field.

2.2 Mechanism of ice flow

In order to derive simplified dynamic/thermodynamics field equations for the large-scale dynamics of ice sheets, Equation (2.2) (momentum balance) is approximated. In the equation, $\boldsymbol{f}$ is set as $\boldsymbol{f} = \rho \boldsymbol{g} = -\rho g \boldsymbol{e}_z$, and the acceleration term in Equation (2.2) is neglected due to small flow velocities (~ 100 m / a) and long time scales (e.g., ≥ 1 ka). Therefore, we obtain for the stresses

$$\frac{\partial t_{xx}}{\partial x} + \frac{\partial t_{xy}}{\partial y} + \frac{\partial t_{xz}}{\partial z} = 0, \tag{2.5}$$

$$\frac{\partial t_{yx}}{\partial x} + \frac{\partial t_{yy}}{\partial y} + \frac{\partial t_{yz}}{\partial z} = 0, \tag{2.6}$$

$$\frac{\partial t_{zx}}{\partial x} + \frac{\partial t_{zy}}{\partial y} + \frac{\partial t_{zz}}{\partial z} = \rho g. \tag{2.7}$$

The ice velocity is calculated from the flow law, which relates the deviatoric stress tensor $\boldsymbol{t}^D$ and the strain-rate tensor $\boldsymbol{D}$ through the following equation,

$$\boldsymbol{D} = EA(T')\sigma^{n-1}\boldsymbol{t}^D, \tag{2.8}$$

where the stress-deviator components $\boldsymbol{t}^D$ are obtained by subtracting the hydrostatic pressure (the mean normal stress) from the stress components,

$$\boldsymbol{t} = -p\boldsymbol{1} + \boldsymbol{t}^D, \qquad p = -\frac{1}{3}\mathrm{tr}\,\boldsymbol{t}. \tag{2.9}$$

By comparing Equation (2.8) with the standard material function of a viscous fluid, we find

$$\boldsymbol{t}^D = 2\eta \boldsymbol{D} \;\Rightarrow\; \frac{1}{\eta} = 2EA(T')\sigma^{n-1}, \tag{2.10}$$

where the coefficient η is called shear viscosity (or simply viscosity), and its inverse $\frac{1}{\eta}$ is the fluidity.

Equation (2.8) is called 'Glen's flow law' (Paterson, 1994), in which the strain rate is proportional to the n-th power of the stress, the ice temperature dependent factor, $A(T')$ (T' is the temperature relative to pressure melting point) and a further factor E. The latter is called enhancement factor, and controls the softness of ice due to the effects of impurity and/or anisotropy. The strain rate is expressed by the spatial derivatives of the velocity components as follows,

$$D_{ij} = \frac{1}{2}\left[\frac{\partial v_i}{\partial x_j} + \frac{\partial v_j}{\partial x_i}\right] \qquad (i, j = x, y, z), \tag{2.11}$$

or explicitly,

$$D_{ij} = \begin{pmatrix} \dfrac{\partial v_x}{\partial x} & \dfrac{1}{2}\left[\dfrac{\partial v_x}{\partial y} + \dfrac{\partial v_y}{\partial x}\right] & \dfrac{1}{2}\left[\dfrac{\partial v_x}{\partial z} + \dfrac{\partial v_z}{\partial x}\right] \\ \dfrac{1}{2}\left[\dfrac{\partial v_y}{\partial x} + \dfrac{\partial v_x}{\partial y}\right] & \dfrac{\partial v_y}{\partial y} & \dfrac{1}{2}\left[\dfrac{\partial v_y}{\partial z} + \dfrac{\partial v_z}{\partial y}\right] \\ \dfrac{1}{2}\left[\dfrac{\partial v_z}{\partial x} + \dfrac{\partial v_x}{\partial z}\right] & \dfrac{1}{2}\left[\dfrac{\partial v_z}{\partial y} + \dfrac{\partial v_y}{\partial z}\right] & \dfrac{\partial v_z}{\partial z} \end{pmatrix}. \qquad (2.12)$$

The effective shear stress σ is defined as the square root of the second invariant of the stress tensor,

$$\sigma = \frac{1}{2}\left[\left(t_{xx}^D\right)^2 + \left(t_{yy}^D\right)^2 + \left(t_{zz}^D\right)^2\right] + t_{xy}^2 + t_{xz}^2 + t_{yz}^2 = \sqrt{\frac{1}{2}\mathrm{tr}\left(\boldsymbol{t}^D\right)^2}\,. \qquad (2.13)$$

Everywhere in an ice sheet except for the immediate vicinity (some 10 km horizontal distance) of ice domes (local maxima of the surface elevation) and ice margins, the flow regime is essentially simple, bed-parallel shear, and the slopes of the free surface and the ice base are small (Figure 8). The horizontal velocity v_x, v_y can be calculated by using Equations (2.5) ~ (2.13) with the stress-free condition at the surface, and simplifications of the stress field called shallow ice approximation (Hutter 1983, Morland 1984).

$$v_x = v_{bx} - 2(\rho g)^n |\mathrm{grad}h|^{n-1} \frac{\partial h}{\partial x} \int_b^z EA(T')(h - \bar{z})^n \, d\bar{z}\,, \qquad (2.14)$$

$$v_y = v_{by} - 2(\rho g)^n |\mathrm{grad}h|^{n-1} \frac{\partial h}{\partial y} \int_b^z EA(T')(h - \bar{z})^n \, d\bar{z}\,. \qquad (2.15)$$

For expressions of the basal velocity (v_{bx}, v_{by}) see below (Section 3.2.1).

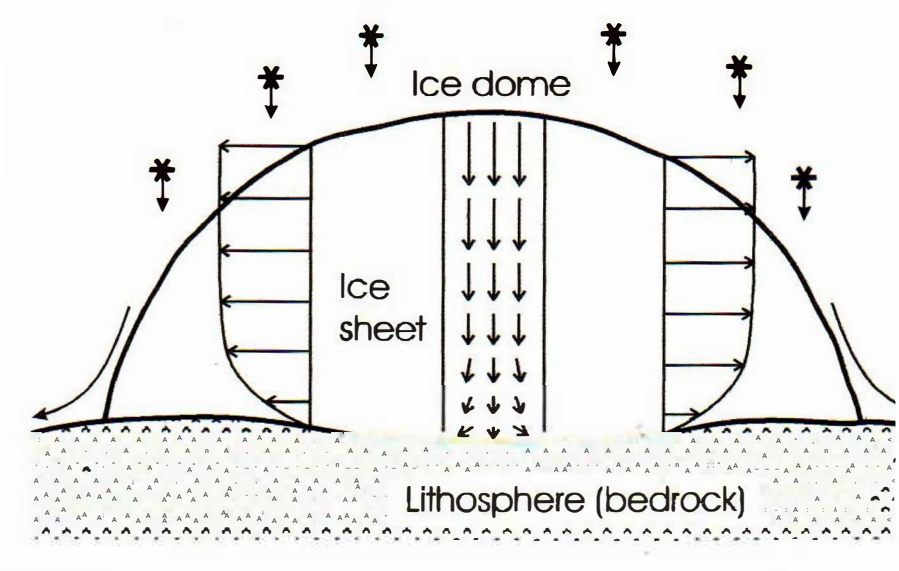

Figure 8. Flow regimes in an ice sheet. (Greve 2004, 2005)

2.3 Temperature equation

The temperature equation can be derived from Equation (2.3) by inserting the constitutive equations for the stress deviator (Equation (2.8)), the heat flux (2.16), and the internal energy (2.17) defined as below,

$$\boldsymbol{q} = -\kappa(T)\mathrm{grad}T\,, \tag{2.16}$$

$$u = \int_{T_0}^{T} c(\overline{T})d\overline{T}\,, \tag{2.17}$$

where κ is the heat conductivity, c the specific heat capacity of ice, and T_0 the melting point at atmospheric pressure, 273.15 K.

Further, except for the very uppermost few centimeters of ice exposed to sunlight, the radiation r is negligible in an ice sheet, so that we obtain the temperature (T) evolution equation as

$$\rho c\frac{dT}{dt} = \mathrm{div}(\kappa\mathrm{grad}T) + 4\eta d^2\,, \tag{2.18}$$

where d the effective strain rate. This is defined as

$$d = \sqrt{\frac{1}{2}\mathrm{tr}\,\boldsymbol{D}^2}\,. \tag{2.19}$$

Evidently, the evolution of the internal temperature field is balanced by diffusion, advection and strain heating.

2.4. Boundary conditions

At the free surface, the kinematic boundary condition is derived as

$$\frac{\partial h}{\partial t} + v_x\frac{\partial h}{\partial x} + v_y\frac{\partial h}{\partial y} - v_z = N_s a_s^{\perp}\,. \tag{2.20}$$

where h represents the free surface, N_s the gradient norm of the surface, $a_s^{\perp}$ the ice volume flux through the free surface which is also known as the accumulation-ablation function or surface mass balance (see Greve, R., 2005b). In addition, the dynamic boundary condition which is related to stresses is

$$\boldsymbol{t}\cdot\boldsymbol{n} = 0\,, \tag{2.21}$$

which describes a stress-free surface. $\boldsymbol{n}$ is the normal unit vector of the surface. For the temperature evolution equation (2.21), it is further required to provide a thermodynamic boundary condition. This can be done with the surface temperature T_s as

$$T = T_s . \tag{2.22}$$

Similar to the free surface, a kinematic boundary condition and the dynamic condition for the ice base can be derived,

$$\frac{\partial b}{\partial t} + v_x \frac{\partial b}{\partial x} + v_y \frac{\partial b}{\partial y} - v_z = N_b a_b^{\perp}, \tag{2.23}$$

$$\boldsymbol{t} \cdot \boldsymbol{n} = \boldsymbol{t}_{lithosphere} \cdot \boldsymbol{n}, \tag{2.24}$$

where b stands for ice the elevation of base adjacent to the bedrock, N_b the gradient norm of the base, $a_b^{\perp}$ the ice volume flux through the base which is called the basal melting rate, $\boldsymbol{t}_{lithosphere}$ the lithospheric stress (Greve, R., (2005b) Dynamics of ice sheets and glaciers). However, since we do not have any information about the stress conditions in the bedrock, an empirical sliding law is required as dynamic boundary condition. In this study, a Weertman-type sliding law is employed, which is described in detail in Section 3.2.1. The thermodynamic boundary condition is expressed in two forms for a cold base and a temperate base. For a cold base, that is, a basal temperature below the pressure melting point, there cannot be any basal melting or sliding, so that

$$\kappa(\mathrm{grad}T \cdot \boldsymbol{n}) = q_{geo}^{\perp}, \tag{2.25}$$

which is a Neumann-type boundary condition for the basal temperature. $q_{geo}^{\perp}$ is the geothermal heat flux which must be prescribed. By contrast, for a temperate base, that is, a basal temperature at the pressure melting point, the basal temperature itself is known,

$$T = T_m, \tag{2.26}$$

which is a Dirichlet-type condition. (See Greve, R., (2005b) Dynamics of ice sheets and glaciers.)

2.5 The evolution of ice thickness

By combining the kinematic boundary conditions of Equation (2.20) and Equation (2.23) with the continuity equation (2.1), we can derive an evolution equation for the ice thickness. The ice thickness is defined as

$$H(x,y,z) = h(x,y,z) - b(x,y,z). \tag{2.27}$$

The schematic picture of a vertical cross section of an ice sheet is shown in Figure 9 (Saito 2002). The components of the mass balance equation (2.1) of an ice sheet are written as

$$\frac{\partial v_x}{\partial x} + \frac{\partial v_y}{\partial y} + \frac{\partial v_z}{\partial z} = 0 . \tag{2.28}$$

Integrating Equation (2.28) from the ice base to the free surface and inserting the kinematic boundary conditions yields

$$\frac{\partial}{\partial x}\int_b^h v_x dz + \frac{\partial}{\partial y}\int_b^h v_y dz + \frac{\partial h}{\partial t} - N_s a_s^{\perp} - \frac{\partial b}{\partial t} + N_b a_b^{\perp} = 0 . \tag{2.29}$$

The volume flux $\boldsymbol{Q}$ is introduced as the vertically integrated horizontal velocity,

$$\boldsymbol{Q} = \begin{pmatrix} Q_x \\ Q_y \end{pmatrix} = \begin{pmatrix} \int_b^h v_x dz \\ \int_b^h v_y dz \end{pmatrix} . \tag{2.30}$$

By using the ice thickness $H = h - b$, we obtain the ice-thickness equation

$$\frac{\partial H}{\partial t} = -\mathrm{div}\,\boldsymbol{Q} + N_s a_s^{\perp} - N_b a_b^{\perp} . \tag{2.31}$$

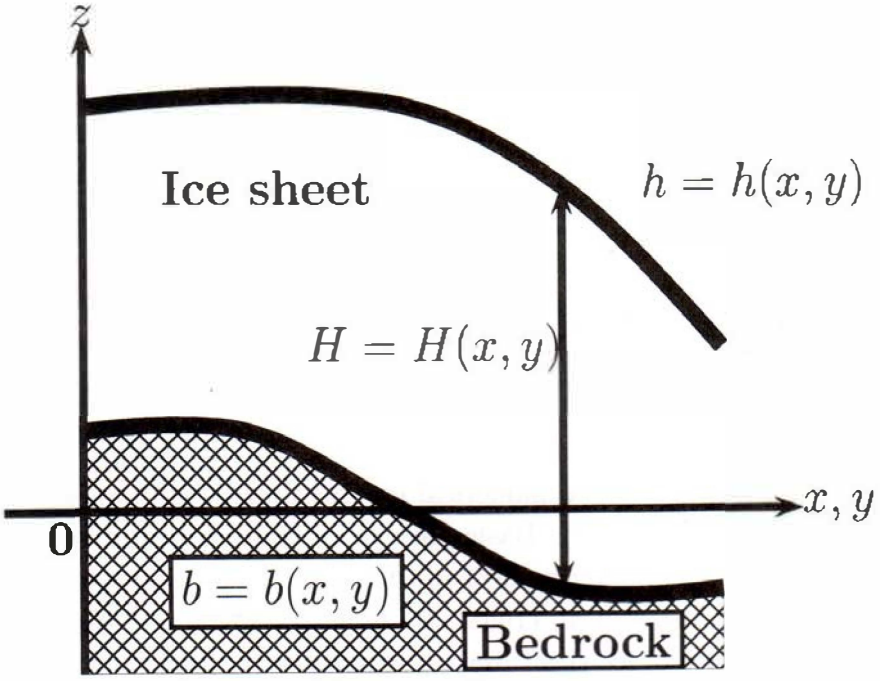

Figure 9. Schematic picture of a vertical cross section of an ice sheet. (Saito 2002)
$h = h(x, y)$ represents the ice surface and $b = b(x, y)$ the ice base adjacent to the bedrock.

3. Model description

3.1 SICOPOLIS

The model SICOPOLIS (Simulation Code for POLythermal Ice Sheets, Greve 1997a, b), is applied to the Greenland ice sheet. SICOPOLIS is a three-dimensional large-scale ice sheet model which is based on the dynamics and thermodynamics of ice sheets. It simulates the extent, thickness, velocity, temperature, water content and age of ice sheets. It is based on the shallow-ice approximation (Hutter 1983, Morland 1984) and the rheology of an incompressible, heat-conducting fluid with Glen's flow law (see Section 2). Temperature and water-content-dependent rate factors are described in detail by Greve et al. (1998), and the isostatic depression and rebound of the lithosphere is modeled by the local-lithosphere-relaxing-asthenosphere (LLRA) with an isostatic time lag (Le Meru and Huybrechts 1996, Greve 2001). The structure of SICOPOLIS is sketched in Figure 10.

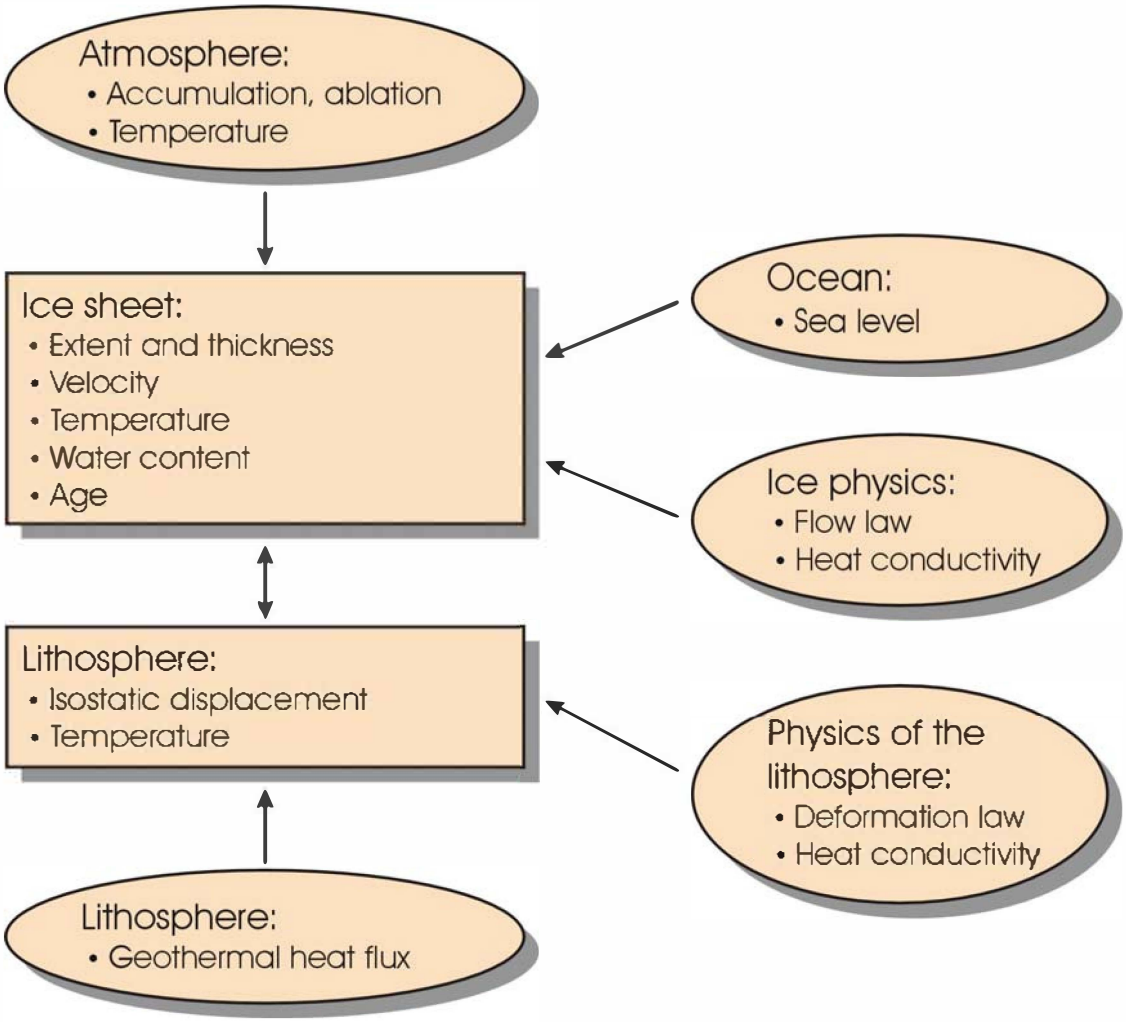

Figure 10. 3D ice sheet model SICOPOLIS (Greve 1997)

3.2 General set-ups

3.2.1 Basal sliding condition

For describing a basal sliding condition, Weertman's theory (Weertman 1957) is used. It explains basal sliding as the motion of ice, passing over bumps on the glacial bed at the melting temperature. According to this theory, ice moves over bedrock bumps by a combination of regelation and enhanced plastic flow (Figure 11). It is reasonable to assume that the ice is frozen to the ground if the basal temperature T_b is below the pressure melting point T_m, so that no-slip conditions prevail. By contrast, if the basal temperature is at pressure melting, basal sliding can be expected and its amount can be related to the basal shear stress $\boldsymbol{\tau}$ and basal overburden pressure P in the form of a power law (Weertman-type sliding law). Therefore, the basal-sliding velocity $\boldsymbol{v}_b$ can be expressed as

$$\boldsymbol{v}_b(T_b') = \frac{C_b e^{T'_b/\gamma_{sms}}}{\rho g} \frac{|\boldsymbol{\tau}|^{p-1}}{P^q} \boldsymbol{\tau} \qquad \text{for } T_b \le T_m \qquad (T'_b \le 0 \ ^\circ\text{C}). \qquad (3.1)$$

The sliding law has been modified to allow for sub-melt sliding via the coefficient $\gamma_{sms} = 1$ ℃ (Hindmarsh and Le Meur 2001, Greve 2005a). Further $\boldsymbol{v}_b$ is the basal sliding velocity, T'_b is the temperature relative to pressure melting, $\boldsymbol{\tau}$ is the basal shear traction between the bed and the ice, ρ is the ice density, g is the gravitational acceleration and $P = \rho g H$ is the over burden pressure. The stress and pressure exponents $p = 3, q = 2$ are suitable for sliding on hard rock and $p = 1, q = 0$ for sliding on soft, deformable sediment (see Greve et al. (2006) and references there in). It has been researched that the bed of Greenland is hard rock (e.g. Bamber et al., 2001b, c), so that the exponents are chosen as $p = 3, q = 2$, and the basal-sliding coefficient is set to $C_b = 10^5$ a^{-1}.

Implementation of the NEGIS is made by the basal sliding condition. In order to produce fast ice flow, the sliding law is modified only in the domain of NEGIS as below,

$$\boldsymbol{v}_b(T_b') = \frac{\widetilde{C}_b e^{T'_b/\gamma_{sms}}}{\rho g} \frac{|\boldsymbol{\tau}|^{p-1}}{P^q} \boldsymbol{\tau}, \qquad (3.2)$$

where $\widetilde{C}_b$ is defined as

$$\widetilde{C}_b = C_b \times m, \qquad m > 1; \qquad (3.3)$$

m is the sliding enhancement factor. Therefore, sliding in the NEGIS area is assumed to be enhanced by the factor m with respect to regular sliding elsewhere.

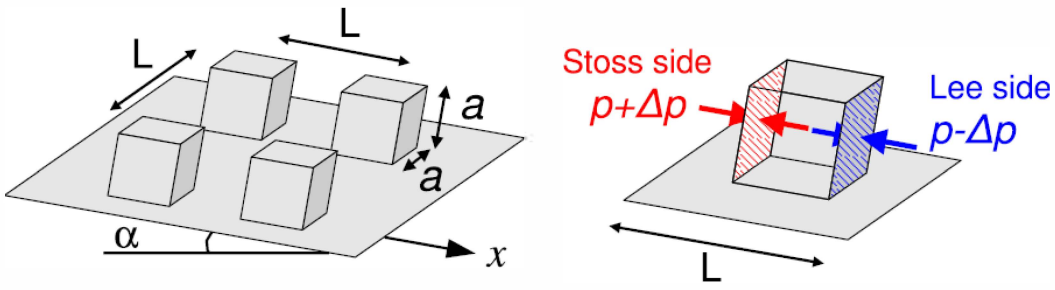

(a) (b)

Figure 11. Schematic diagram of Weertman-type sliding showing (a) periodically distributed bed bumps and (b) pressure perturbation at the stoss and lee sides of bumps (Sugiyama 2006). 'L' is the distance of each bump, and 'a' a side of a bump, 'α' the slope of the bed plane. Ice melts when the pressure intensifies in stoss sides at the pressure melting point, and refreezes in less sides where the pressure is smaller.

3.2.2 Paleoclimatic forcing

In order to calculate the paleoclimatic forcing, a glacial index $g(t)$ is introduced. The glacial index is used to determine the surface-temperature and precipitation distribution over the ice sheet by interpolation between present and LGM conditions. The source of the index is based on the $\delta^{18}O$ record of GRIP (Dansgaard et al. 1993), which is a proxy for the surface-temperature history of the Greenland ice sheet (Johnsen et al., 1995). Before 105 ka BP, due to the falsification of ice core record by irregular ice flow, the surface-temperature history derived from δ D of the Antarctic Vostok ice core (Petit et al. 1999) is used instead. The glacial index is defined as follows,

$$g(t) = \frac{T_s(t) - T_{s,present}}{T_{s,LGM} - T_{s,present}}, \tag{3.4}$$

and the reference values are

$$T_{s,present} = -31.74\,℃ \text{ (for } \delta^{18}O = -35.2\ ‰), \tag{3.5}$$

$$T_{s,LGM} = -55.15\ ℃ \text{ (for } \delta^{18}O = -42.71\ ‰), \tag{3.6}$$

where the latter represents the LGM minimum taken at 21.9 ka BP. The glacial index is shown in Figure 12.

The glacial index $g(t)$ is defined such that $g = 1$ for LGM conditions and $g = 0$ for present conditions (Forsström et al. 2003, Forsström and Greve 2004). The present-day surface air temperature is parameterized following Ritz et al. (1997), and the present precipitation is constructed based on the digitized accumulation map by Calanca et al. (2000). LGM climate is the results from GCM simulations with the UKMO model (Hewitt and Mitchell 1997), which were carried out for the Paleoclimate Modeling Intercomparison Project (PMIP, www-lsce.cea.fr/pimp). The climate conditions referred to $g(t)$ at any time t in the runs are obtained by weighting the interpolation between present-day climate conditions and LGM climate conditions.

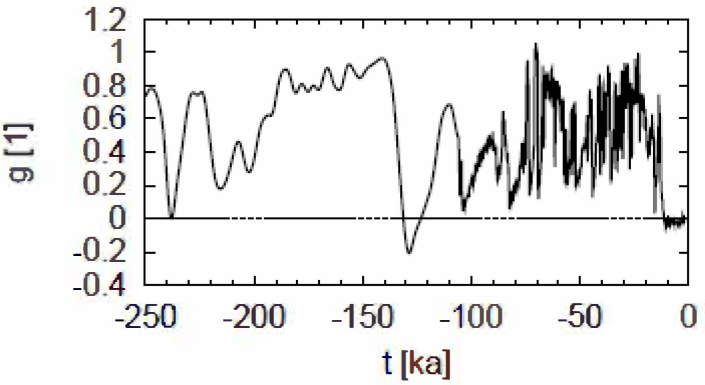

Figure 12. Glacial index $g(t)$ derived from the GRIP and Vostok surface-temperature records (Dansgaard et al. 1993, Johnsen et al. 1995, Petit et al. 1999).

3.2.3 Future climatic forcing: WRE scenarios

In the future simulations, WRE scenarios are used as global warming climatic forcings. They were originally based on the scenarios developed by Wigley, Richels and Edmonds (1996). Working Group I (WGI) of the IPCC (Intergovernmental Panel on Climate Change) developed a set of illustrative pathways for stabilizing the atmospheric CO_2 concentration at 350, 450, 550, 650 and 750 ppm (Enting et al. 1994, Schimel et al. 1995). Wigley, Richels and Edmonds constructed the WRE scenarios from the WGI profiles which were devised with corresponding anthropogenic emissions requirements. The WRE scenarios were improved by Cubasch et al. (2001) in the second assessment report of IPCC, and the new scenarios were derived from WRE profiles under the assumption of stabilization of the atmospheric CO_2 concentration at 450, 550, 650, 750 and 1000 ppm, respectively. The associated global mean temperatures are derived from average values which were calculated by nine different GCM's driven by the WRE profiles (Cubasch et al., 2001).

Church et al. (2001) reported the 21st century's temperature change as the results of the IS92a scenario with nine different AOGCM experiments. In the report, the change of temperature over the Greenland ice sheet was in the range of 1.3 to 3.1 times the global mean change, with an average ratio of approximately 2, which is used in this study. The increase in precipitation over Greenland was in the range of 2.7 to 7.8 % / ℃ with an average of approximately 5 % / ℃, and again the latter value is used here. Figure 13 shows the CO_2 concentration of each scenarios, and Figure 14 the global surface temperature change.

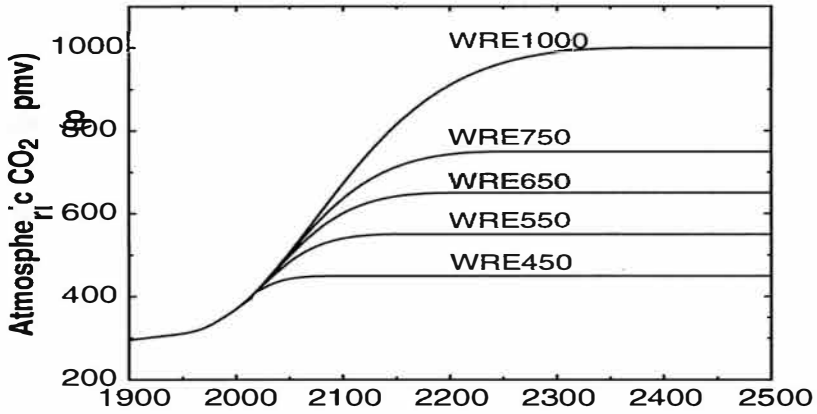

Figure 13. WRE profiles which assume stabilization of atmospheric CO_2 concentration for at 450, 550, 650, 750 and 1000 ppm, respectively.
(Cubasch et al., 2001)

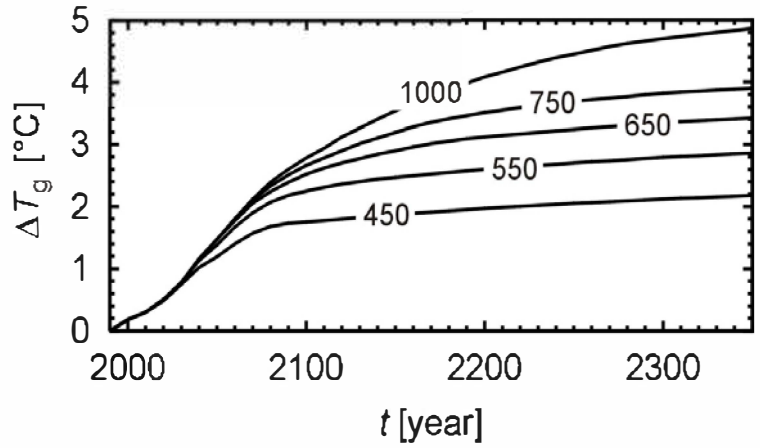

Figure 14. Global mean temperature change ΔT_g for the profiles WRE450, WRE550, WRE650, WRE750and WRE1000 (stabilization scenarios for atmospheric CO_2), by Cubasch et al. (2001).

3.2.4 Surface meltwater

In order to calculate the amount of meltwater, a positive degree-day (PDD) model (Reeh 1991) is used, which is a parameterization for the melt rate of snow and ice at surface of an ice sheet or glacier. It is based on the assumption that melt rate is proportional to the surface air temperature excess above 0 ℃ (e.g. Braithwaite and Olesen, 1989, Hock 2003). The positive degree days (PDD) are computed following Calov and Greve (2005),

$$PDD = \int_0^A dt \left\{ \frac{\sigma}{2\pi} \exp\left(-\frac{T_{ac}^2}{2\sigma^2} \right) + \frac{T_{ac}}{2} \operatorname{erfc}\left(-\frac{T_{ac}}{\sqrt{2}\sigma} \right) \right\}, \tag{3.7}$$

where T_{ac} is the annual temperature cycle, σ is the standard deviation of the temperature from the annual cycle, erfc is error function and $A = 1$ year. The PDD model yields for the melting rate

$$M = \max\left[\beta_{ice} \left(\frac{PDD}{\Delta t_m} - \frac{P_{max} S}{\beta_{snow}} \right),\ 0 \right], \tag{3.8}$$

where M is the melting rate, PDD are the positive-degree days during the melting season of duration Δt_m, S is the solid precipitation (snowfall rate), and the degree-day factors for ice melt and snow melt are β_{ice} and β_{snow}, respectively. The saturation factor for the formation of superimposed ice is P_{max} (Greve 2005a).

With a view to introduce the effect of surface meltwater on basal sliding, the Weertman-type sliding law of Equation (3.1) is modified as follows,

$$\boldsymbol{v}_b(T_b') = \frac{C_{b,smw} e^{T'_b/\gamma_{sms}}}{\rho g} \frac{|\boldsymbol{\tau}|^{p-1}}{P^q} \boldsymbol{\tau}, \tag{3.9}$$

where $C_{b,smw}$ is the basal sliding coefficient including the surface maltwater effects, defined as

$$C_{b,smw} = C_b(1 + \gamma M). \tag{3.10}$$

The parameter γ is the surface meltwater coefficient. For the NEGIS area, the basal sliding coefficient

$$\widetilde{C}_{b,smw} = C_b m(1 + \gamma M), \tag{3.11}$$

which includes the sliding enhancement factor m, is used instead.

Here we estimate the value of the surface meltwater coefficient γ by data from Zwally et al. (2002). By subtracting the new basal sliding law of Equation (3.9)

from the original basal sliding law of Equation (3.1), the difference of

$$\Delta v_b = \frac{C_b \gamma M}{\rho g} \frac{\tau_b^3}{p_b^2} \tag{3.12}$$

can be attributed to meltwater-induced acceleration. If we employ the relations

$$p_b = \rho g H \,, \quad \tau_b = \rho g H \,|\nabla h\,|, \tag{3.13}$$

the difference Δv_b in Equation (3.12) can be written as

$$\Delta v_b = C_b \gamma M H \,|\nabla h\,|^3 . \tag{3.14}$$

For the Swiss Camp in central west Greenland, Zwally et al. (2002). reported a value of $PDD = 116.5$ ℃d for the summer melting season ($\Delta t_m \approx 120$ d) in 1998. With the snowfall rate $S \approx 220$ mm w.e. /a ≈ 0.6 mm w.e. /d (Ohmura and Reeh 1991), Equation (3.12) yields a melting rate of $M \approx 6$ mm w.e. /d ≈ 6.5 mm i.e. /d. The increase of ice-flow velocity during the summer of 1998 was 88 mm /d (Zwally et al. 2002). If this increase is identified with the meltwater-induced acceleration of basal sliding Δv_b, Equation (3.14) can be solved for the coefficient γ as,

$$\gamma = \frac{\Delta v_b}{C_b M H \,|\nabla h\,|^3} . \tag{3.15}$$

With the ice thickness $H = 1220$ m and the surface slope $|\nabla h| \approx 0.01$ (Parizek and Alley 2004), this yields a value for the surface-meltwater coefficient of $\gamma \approx 0.11$ a / m.

Note that this estimate holds only for one particular position in the ice sheet. Therefore, it is not necessarily representative for the NEGIS area or the entire ice sheet, and a suitable overall value may differ from this estimate substantially.

3.2.5 Other physical parameters

The standard physical parameters of the ice-sheet model SICOPOLIS are listed in table 1. Note that $E = 1$ holds for Holocene or Eemian ice (deposited between 11 ka BP and the present, or between 132 and 114.5 ka BP), and $E = 3$ holds for Weichselian or pre-Eemian ice (deposited during other times).

Quantity	Value
Gravity acceleration, g	9.81 m / s^2
Density of ice, ρ	910 kg / m^3
Power-law exponent, n	3
Flow-enhancement factor, E	1 / 3 *
Melting point at atmospheric pressure, T_0	273.15 K
Heat conductivity of ice, κ	9.828 $e^{-0.0057T[K]}$W / m K
Specific heat of ice, c	(146.3 + 7.253 T[K])J / kg K
Latent heat of ice, L	335 kJ / kg
Clausius-Clapeyron gradient, β	8.7×10^{-4} K / m
Isostatic time lag, τ_{iso}	3000 a
Asthenosphere density, ρ_a	3300 kg /m
Density specific × heat of the lithosphere, $\rho_r c_r$	2000 kJ / m^3 K
Heat conductivity of the lithosphere, κ_r	3 W / m K

Table1. Standard physical parameters of the ice-sheet model SICOPOLIS. (Greve 2005a)

(* See main text.)

4. Paleoclimatic simulations

4.1 Set-up of GRL20: 20 km grid

The first part of the paleoclimatic simulations are carried out with a 20-km resolution grid, and these experiments are referred to as GRL20 runs. The horizontal grid leads to 82 by 140 grid points in the stereographic plane, and in the vertical, 81 grid points in the cold ice region, 11 grid points in the temperate region and 11 grid points in the lithosphere are used. The model domain follows the previous work by Greve (2005a) which covers entire Greenland with the surrounding sea, and the domain map of the NEGIS area is determined by Figure 15 (Contour plot of balance velocities up to 500 m / a). Model time is from 250 ka BP until the present (0 ka), and spin-up simulations are from 422 ka BP until 250 ka BP. The time step for all model components is 5 a.

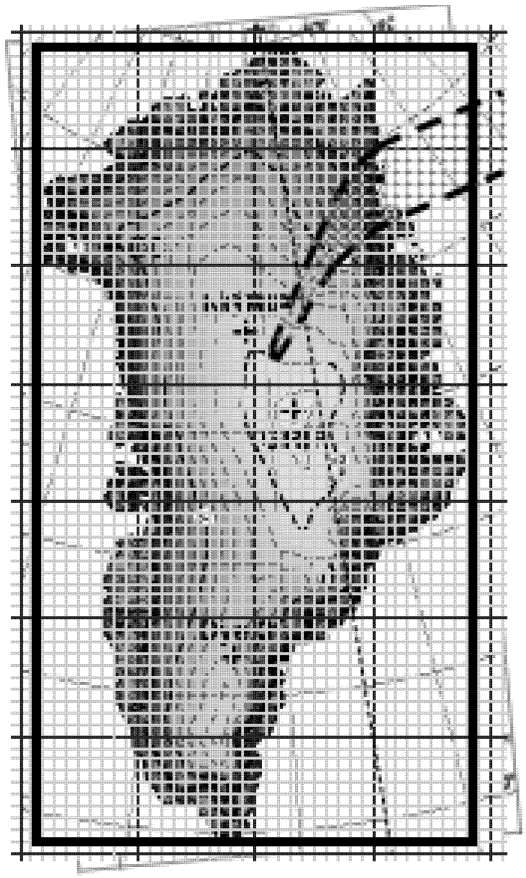

Figure 15. The domain map of NEGIS based on the Figure 5 (contour plot of balance velocities up to 500 m / a by Bamber et al., 2001a) in 40-km resolution. NEGIS is represented within black broken lines and orange plots are the NEGIS area simulated in the runs.

4.1.1 Results and discussion of the reference simulation without the NEGIS (GRL20_REF)

As first experiment, a reference run without the NEGIS is carried out. This simulation carefully follows the previous work by Greve (2005a), with a distribution of the geothermal heat flux based on the heat flux data set of Pollack et al. (1993). Geothermal heat fluxes were further modified, such that the simulated basal temperatures match the measured ones at the location of four deep ice cores, GRIP (Greenland ice core project), NorthGRIP (NGRIP), Camp Century (CC) and Dye 3.

Figure 16(a), Figure 17(a), and Figure 18(a) show the results of surface elevation, surface velocity, and ice-thickness deviation (difference of simulated results and observed data) of the reference simulation. In the surface elevation map, brown areas represent ice free areas, and blue areas are ice covered. In the surface velocity map, dark red areas show velocities faster than 1000 m / a, and the ice thickness deviation is smaller when the contour is pale blue or beige. Compared to the observed present-day ice thickness, the resulting ice thickness is 1.2 % too large at GRIP, 1.1 % too small at NGRIP, 4.9 % too small at Camp Century and 11.9 % too small at Dye 3. As a meaningful comparison, Figure 17(f) shows the observed surface-velocity data of the NEGIS area, which were researched as part of the Program for Arctic Regional Climate Assessment (PARCA) [Data sets from "Data and Information Service for CliC" (http://clic.npolar.no/disc/), courtesy Dr. Ian Joughin].

4.1.2 Results and discussion of simulations with varied basal sliding coefficient (GRL20_ BSC)

In order to account for the NEGIS, enhanced basal sliding is now introduced to the model. Refering to the balance velocities by Bamber et al. (2001b, c), the NEGIS area is placed in the domain map (Figure 15). The coefficient of the Weertman-type sliding law (3.3) is used. In Equation (3.4), the basal sliding coefficient $\widetilde{C}_b$ is changed with the sliding enhancement factor $m = 2$ (GRL20_BSC2), $m = 5$ (GRL20_BSC5), $m = 10$ (GRL20_BSC10), $m = 20$ (GRL20_BSC20).

Figure 16(b) ~ (e), Figure 17(b) ~ (e), and Figure 18(b) ~ (e) show the results of surface elevation, surface velocity, and ice-thickness deviation for these experiments. In the surface elevation maps of Figure 16(b) ~ (e), the elevations in the NEGIS area decrease, and the ice covered areas retreat with increasing m. It also can be seen that the contour lines are bended toward the inland in the north-east. Surface velocities show red areas whose velocity is over 300 m / a for the runs with m larger than 5, and

these results better reproduce to the observed PARCA data (Figure 17 (f)). Surface elevation changes are more visible in the results of ice-thickness deviations. Surface lowering is evident as m increases, and GRL20_BSC10 and GRL20_BSC20 lead to too thin ice in the NEGIS area with misfits of - 200 m. The GRL20_BSC2 ($m = 2$) result shows a good agreement, with values of ice thickness deviations, within ± 50 m.

From the GRL20_BSC runs we cam see that varying the basal sliding coefficient shows a very clear effect on the NEGIS. Ice-thickness deviations provide a reasonable value for a sliding enhancement factor $m = 2$. From the surface-velocity results of the NEGIS, a factor m larger than 2 provides the best fit when compared to the contour plot of balance velocities by Bamber et al. (2001) (Figure 5) or to the observed data by PARCA (Figure 17(f)). The discrepancy of the best-fitting m between the results of ice thickness and surface velocity may suggest that the NEGIS does not exist during the whole period of the simulations. It may present or appear stronger in warmer eras while being less significant in colder eras due to coldness of the surrounding environment and increased stiffness of the ice.

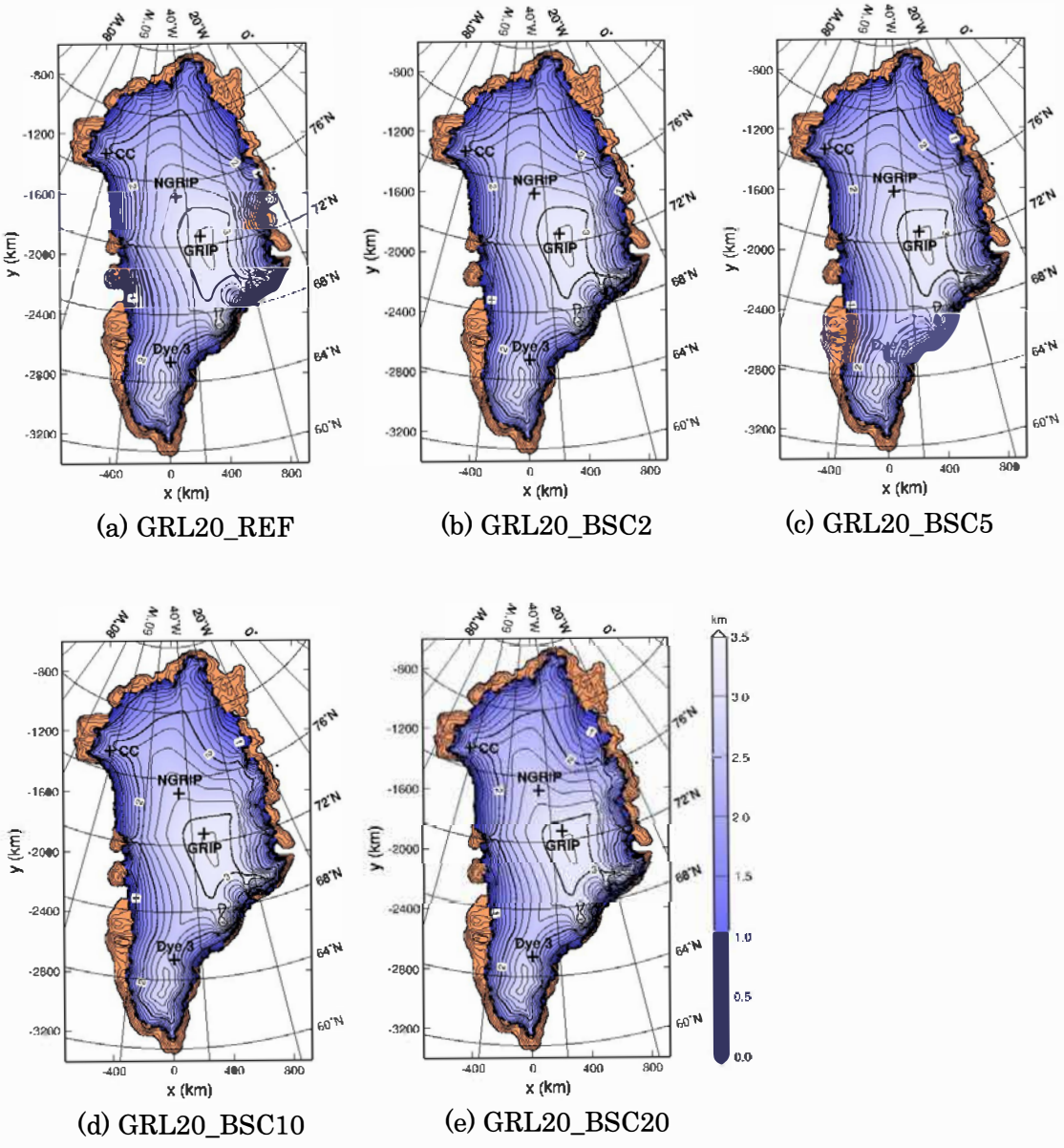

(a) GRL20_REF (b) GRL20_BSC2 (c) GRL20_BSC5

(d) GRL20_BSC10 (e) GRL20_BSC20

Figure 16. Results of surface elevation of varied basal sliding coefficient in 20-km resolution.

(a): GRL20_REF, reference simulation without the NEGIS.

(b): GRL20_BSC2, $m = 2$ at NEGIS.

(c): GRL20_BSC5, $m = 5$ at NEGIS.

(d): GRL20_BSC10, $m = 10$ at NEGIS.

(e): GRL20_BSC20, $m = 20$ at NEGIS.

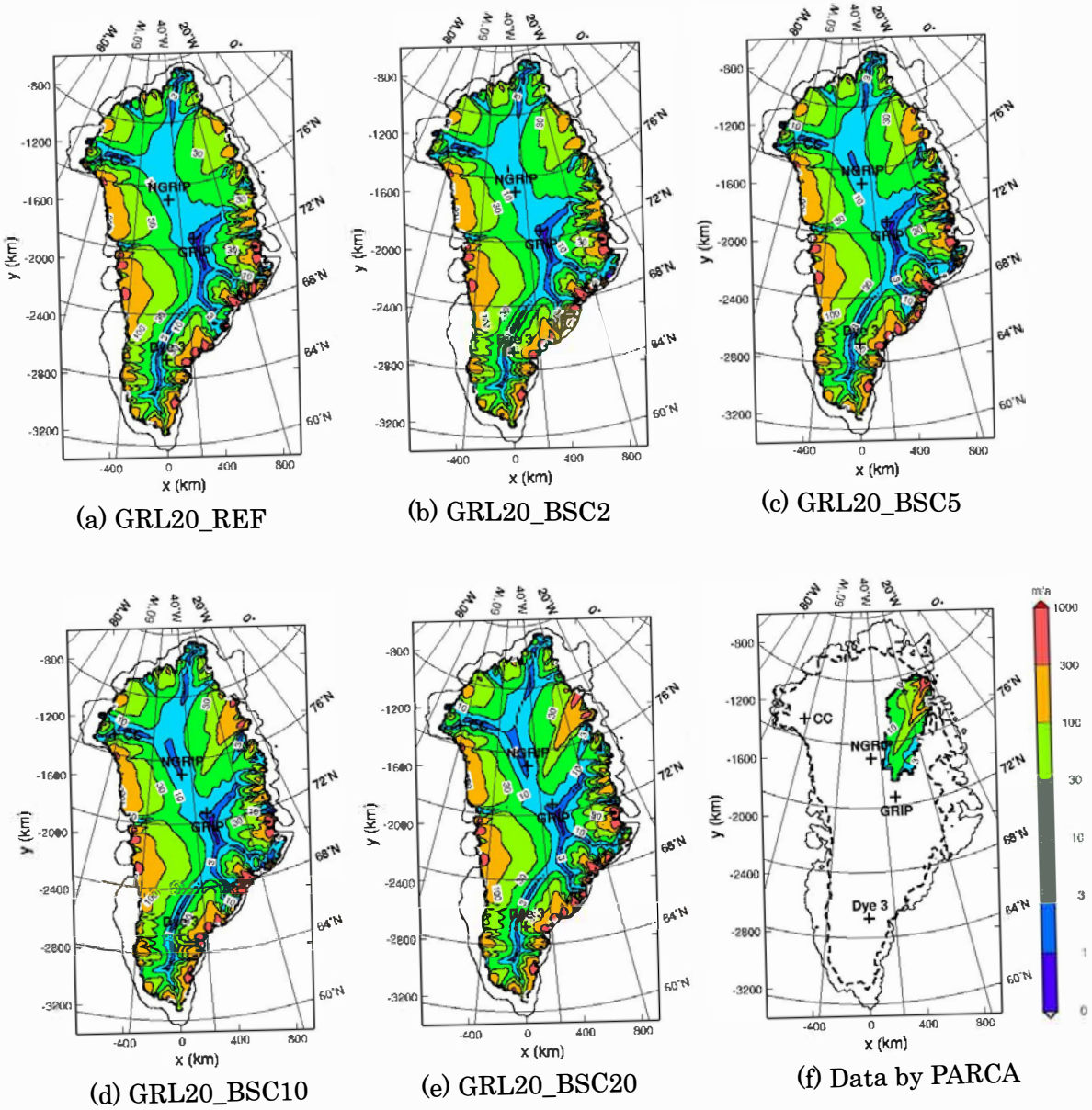

Figure 17. Results of surface velocity of varied basal sliding coefficient in 20-km resolution.

(a): GRL20_REF, reference simulation without the NEGIS.

(b): GRL20_BSC2, $m = 2$ at NEGIS.

(c): GRL20_BSC5, $m = 5$ at NEGIS.

(d): GRL20_BSC10, $m = 10$ at NEGIS.

(e): GRL20_BSC20, $m = 20$ at NEGIS.

(f): Observed surface velocity in the NEGIS area (data by PARCA, courtesy Dr. Ian Joughin).

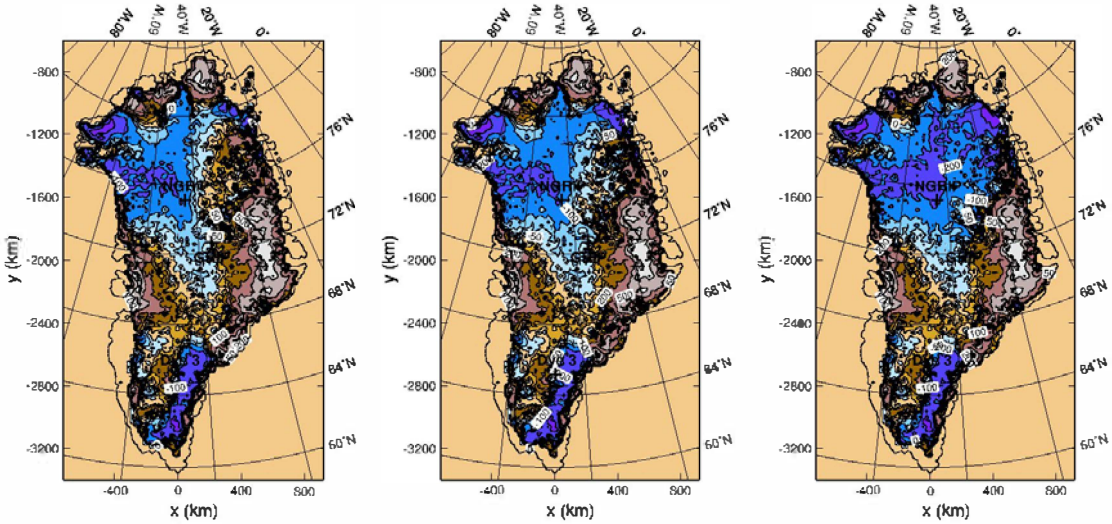

(a) GRL20_REF (b) GRL20_BSC2 (c) GRL20_BSC5

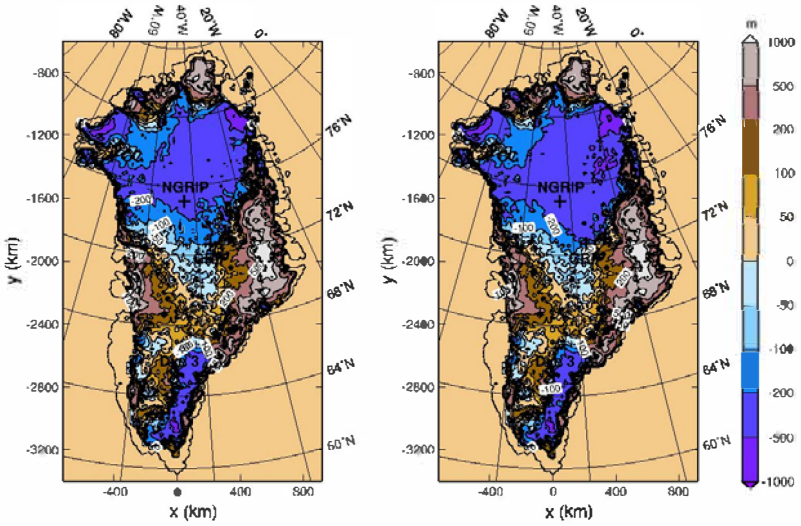

(d) GRL20_BSC10 (e) GRL20_BSC20

Figure 18. Results of ice-thickness deviation of varied basal sliding coefficient in 20-km resolution.

(a): GRL20_REF, reference without the NEGIS.

(b): GRL20_BSC2, $m = 2$ at NEGIS.

(c): GRL20_BSC5, $m = 5$ at NEGIS.

(d): GRL20_BSC10, $m = 10$ at NEGIS.

(e): GRL20_BSC20, $m = 20$ at NEGIS.

4.1.3 Results and discussion of simulations with varied surface meltwater coefficient (GRL20_SMW)

In these simulations, the effect of surface meltwater on the basal sliding speed is investigated. The NEGIS area is placed in the same domain as for the GRL20_BSC runs, and Equation (3.11) is used as the basal boundary condition in the NEGIS area. That is, enhancement of basal sliding via the factor m is not taken into account. As I mentioned previously, the production of surface meltwater is calculated by means of the positive degree-day model. Since the estimated value for the surface meltwater coefficient γ 0.1 a / m in Equation (3.15) is too small to detect the effects of the meltwater on the ice sheet, the surface meltwater coefficient γ in Equation (3.11) is varied as 1 a / m (GRL20_SMW1), 2 a / m (GRL20_SMW2), 3 a / m (GRL20_SMW3), 4 a / m (GRL20_SMW4), 5 a / m (GRL20_SMW5), and 6 a / m (GRL20_SMW6).

Figure 19(a) ~ (f), Figure 20(a) ~ (f), and Figure 21(a) ~ (f) show the results of these simulations for surface elevation, surface velocity, and ice-thickness deviation, respectively. It is difficult to find clear differences in the surface elevation maps; however, the ice-thickness deviations show notable lowerings at NEGIS margins in GRL20_SMW1 to GRL20_SMW3, and the difference becomes more distinct even further inland in GRL20_SMW4 to GRL20_SMW6. From the surface-velocity results, comparison to the contour plot of balance velocities by Bamber et al. (Figure 5) and the observed data by PARCA (Figure 17(f)) demonstrates that the variation of γ affects the surface velocities only near the margins even for the largest value of $\gamma = 6$ m / a (60 times larger than the estimate).

These results show that the surface meltwater has a significant effect on ice flow only near the ice margins, and its influence on the overall ice volume is very small. Therefore, the surface meltwater effect itself cannot explain the onset of the NEGIS as far upstream as observed. This is so because the inland is too cold to produce large amounts of meltwater, which mainly occurs in the vicinity of the ablation areas close to the ice margin.

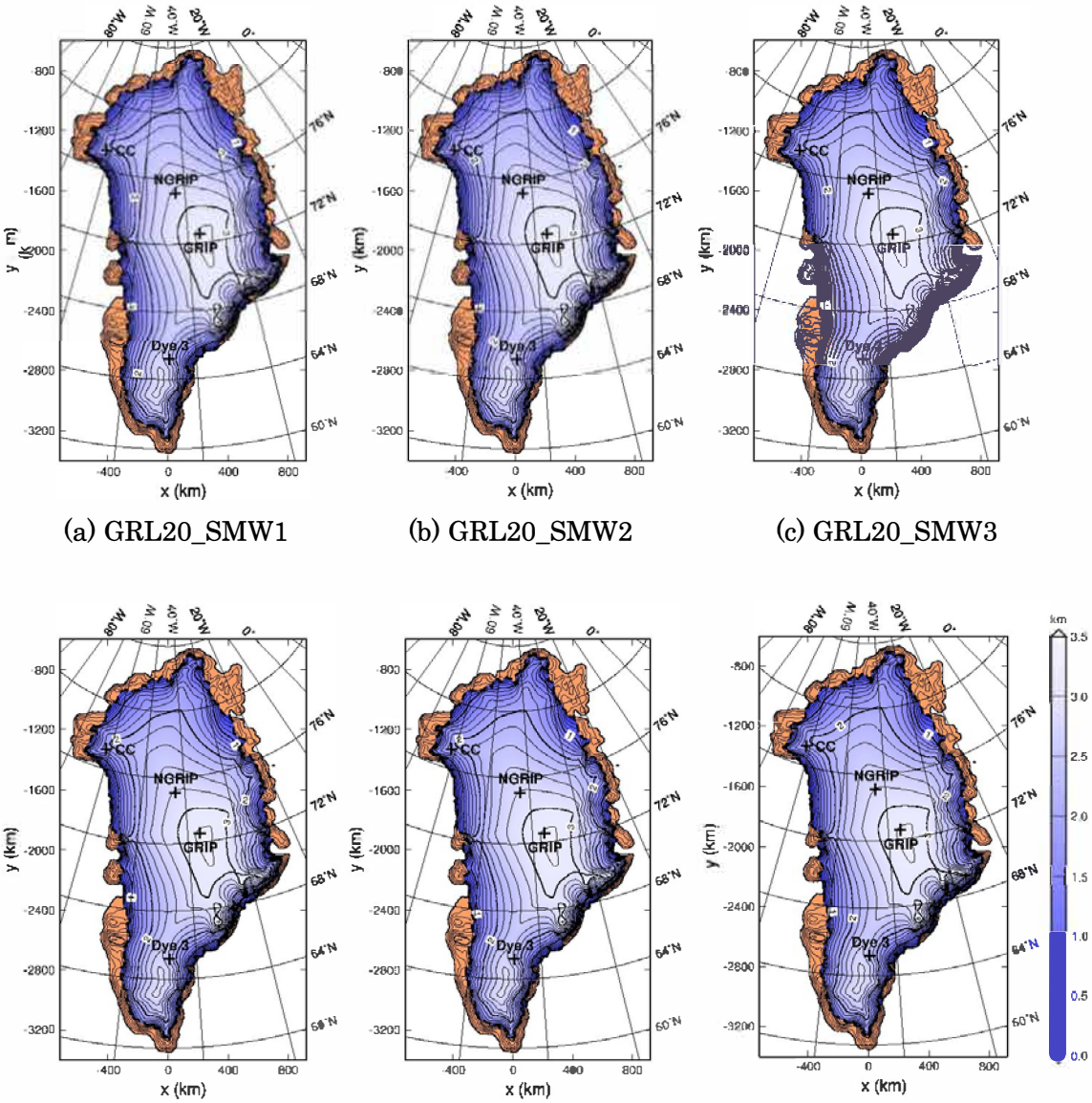

(a) GRL20_SMW1 (b) GRL20_SMW2 (c) GRL20_SMW3

(d) GRL20_SMW4 (e) GRL20_SMW5 (f) GRL20_SMW6

Figure 19. Results of surface elevation of varied surface meltwater coefficient in 20-km resolution.

(a): GRL20_SMW1, γ = 1 a / m at NEGIS.

(b): GRL20_SMW2, γ = 2 a / m at NEGIS.

(c): GRL20_SMW3, γ = 3 a / m at NEGIS.

(d): GRL20_SMW4, γ = 4 a / m at NEGIS.

(e): GRL20_SMW5, γ = 5 a / m at NEGIS.

(f): GRL20_SMW6, γ = 6 a / m at NEGIS.

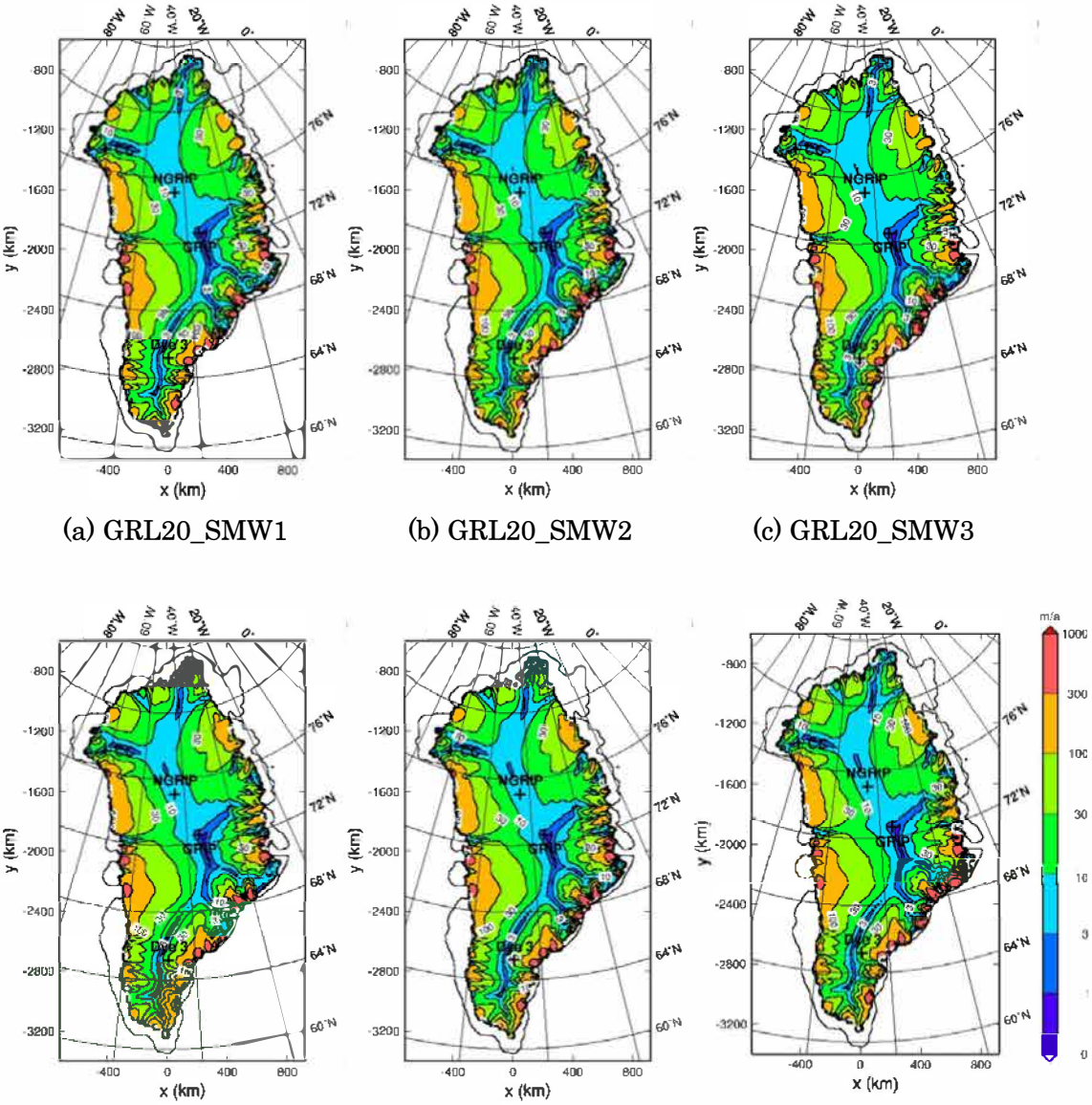

(a) GRL20_SMW1 (b) GRL20_SMW2 (c) GRL20_SMW3

(d) GRL20_SMW4 (e) GRL20_SMW5 (f) GRL20_SMW6

Figure 20. Results of surface velocity of varied surface meltwater coefficient in 20-km resolution.

(a): GRL20_SMW1, γ = 1 a / m at NEGIS.

(b): GRL20_SMW2, γ = 2 a / m at NEGIS.

(c): GRL20_SMW3, γ = 3 a / m at NEGIS.

(d): GRL20_SMW4, γ = 4 a / m at NEGIS.

(e): GRL20_SMW5, γ = 5 a / m at NEGIS.

(f): GRL20_SMW6, γ = 6 a / m at NEGIS.

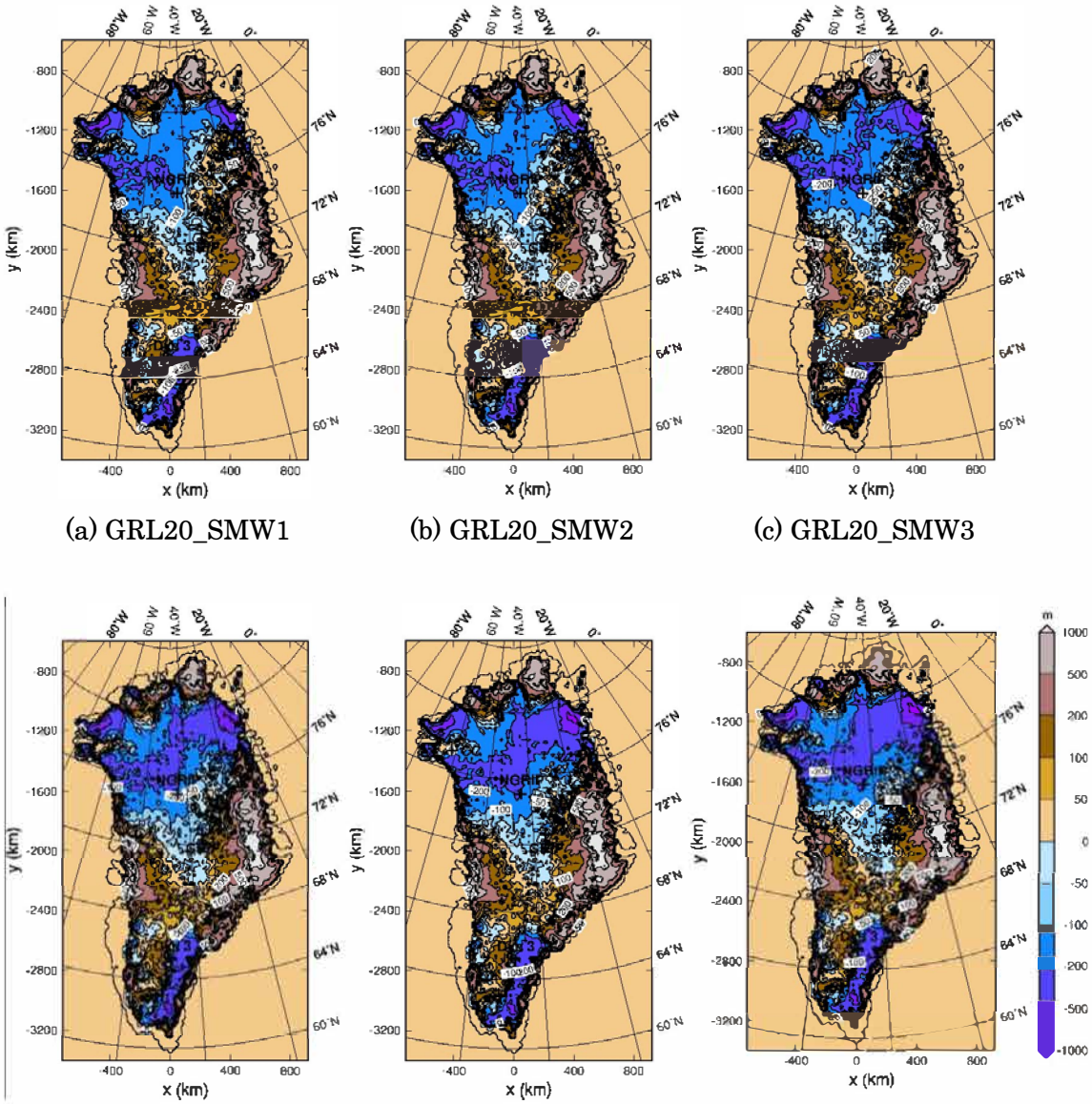

(a) GRL20_SMW1 (b) GRL20_SMW2 (c) GRL20_SMW3

(d) GRL20_SMW4 (e) GRL20_SMW5 (f) GRL20_SMW6

Figure 21. Results of ice-thickness deviation of varied surface meltwater coefficient in 20-km resolution.

(a): GRL20_SMW1, γ = 1 a / m at NEGIS.

(b): GRL20_SMW2, γ = 2 a / m at NEGIS.

(c): GRL20_SMW3, γ = 3 a / m at NEGIS.

(d): GRL20_SMW4, γ = 4 a / m at NEGIS.

(e): GRL20_SMW5, γ = 5 a / m at NEGIS.

(f): GRL20_SMW6, γ = 6 a / m at NEGIS.

4.1.4 Conclusion of GRL20 and motivation for next simulations

In the GRL20_BSC simulations, there is a disagreement to determine the basal sliding coefficient between the results of the ice-thickness deviation and the surface velocity at the NEGIS. The best-fitting value of the sliding enhancement factor is $m = 2$ from the maps of the ice-thickness deviation, which produces the smallest deviation among the simulations. On the other hand, the maps of surface velocity show that the value of $m = 2$ is too small, concluded by comparisons to the contour plot of balance velocities by Bamber et al. (2001) (Figure 5) and the observed data by PARCA (Figure 17(f)).

In an attempt to resolve this discrepancy, the effect of the surface melt-water has been introduced in the GRL20_SMW simulations. The idea of surface melt-water relies on the assumption that the surface melt-water penetrates quickly and affects the basal condition much faster than geothermal and climatic heat conductivity. However, the results of the GRL20_SMW show that the effect of surface meltwater on ice volume change is significant only at the margins where the surface temperature is warm enough to produce sufficient meltwater. Therefore it cannot explain the onset of the NEGIS as far upstream as observed. This outcome must be solved by improving and adding new ideas to the model.

4.2 Set-up of GRL10: 10 km grid

In order to investigate the NEGIS more precisely and evaluate the discrepancy of the sliding enhancement factor m in GRL20 runs, as the second part of the paleoclimatic simulations the GRL10 runs are carried out with a horizontal resolution of 10 km, which leads to 164 by 280 grid points. The vertical grid is the same as for the GRL20 runs, and the model domain of NEGIS is changed following the description of Fahnestock et al. (1993) in the purpose of getting a more detailed representation of the NEGIS. Model time is from 127 ka BP until the present (0 ka), and the initial conditions are derived from a single spin-up simulation in order to save computing time. The initial conditions were well tuned by the distribution of the geothermal heat flux on the ice sheet, using the basal temperature data of the deep ice cores. (See the reference data of the temperatures and ice thickness data in Greve 2005a.) Time step for all model components is 1 a.

4.2.1 Result and discussion of the reference simulation without the NEGIS (GRL10_REF)

Like simulation GRL20_REF, the reference run GRL10_REF is carried out without the NEGIS. The basal sliding coefficient in Equation (3.1) is set, and the rest of the settings of climatic forcing are the same as in GRL20_REF. For the GRL10 simulations, scatter plots are used as a more objective tool for the evaluation of deviations of ice thickness and surface velocity. Two types of scatter plots are created; 1. for the mean of misfit, and 2. for the RMS (root mean square) of misfit. Mean and RMS misfit are defined as below,

$$Mean = \frac{\sum_{i,j} H_{sim}(i,j) - H_{obs}(i,j)}{N}, \tag{4.1}$$

$$RMS = \sqrt{\frac{\sum_{i,j} \{H_{sim}(i,j) - H_{obs}(i,j)\}^2}{N}}. \tag{4.2}$$

The mean and RMS are computed for the misfits in ice thickness and surface velocity, respectively.

Figures 22(a), 23(a), and 24(a) show the resulting surface elevation, surface velocity, and ice-thickness deviation, respectively. Also, the scatter plots of ice thickness and surface velocity are shown in Figure 25(a) and Figure 26(a), respectively. From the scatter plots, we find that the simulated ice-thickness deviations are larger than the observed ones (Figure 25(a)), and the simulated surface velocities are slower than the observed ones (Figure 26(a)). Both results of scatter plots suggest that the ice flow is too slow in NEGIS area, and therefore the basal sliding at NEGIS must be corrected to reproduce the observational feature.

4.2.2 Results and discussion of simulations with varied basal sliding coefficient for non-linear basal sliding (GRL10_ BSC)

Like it was done in GRL20_BSC, the sliding enhancement factor m in Equation (3.3) is varied as $m = 2$ (GRL10_BSC2), $m = 3$ (GRL10_BSC3), $m = 4$ (GRL10_BSC4), $m = 5$ (GRL10_BSC5), and the stress and pressure exponents are chosen as $p = 3, q = 2$ (non-linear basal sliding).

Figures 22(b) ~ (e), 23(b) ~ (e), and 24(b) ~ (e) show the results for the surface elevation, surface velocity, and ice-thickness deviation, respectively. Also, the scatter plots of ice thickness and surface velocity are shown in Figures 25(b) ~ (e) and 26(b) ~ (e), respectively. The surface elevations show that the contour lines bend toward the

summit with increasing m (Figure 22(b) ~ (e)), similar to GRL20_BSC runs. The ice-thickness deviations (Figure 23(b) ~ (e)) are smallest deviations in GRL10_BSC2 and GRL10_BSC3. As for the surface velocities, the red areas whose velocity is over 300 m / a appear in the runs with a factor m larger than 2. The scatter plots of ice thickness show that the minimum of 'mean of misfit' is + 11.20 m in GRL10_BSC2 ($m = 2$), and the minimum of 'RMS of misfit' is 137.1 m in GRL10_BSC3 ($m = 3$) (Table 2). On the other hand, for the surface velocity of ice, the minimum of 'mean of misfit' is – 0.883 m / a in GRL10_BSC4 ($m = 4$), and the minimum of 'RMS of misfit' is 66.52 m / a in GRL10_BSC3 ($m = 3$) (Table 3). Moreover, in the scatter plots in GRL10_BSC3, points fall nicely on the line which represents the minimum deviation. From these results, it is concluded that the most proper value of the sliding enhancement factor is $m = 3$, that is, basal sliding in the NEGIS area is three times more pronounced that elsewhere in the ice sheet.

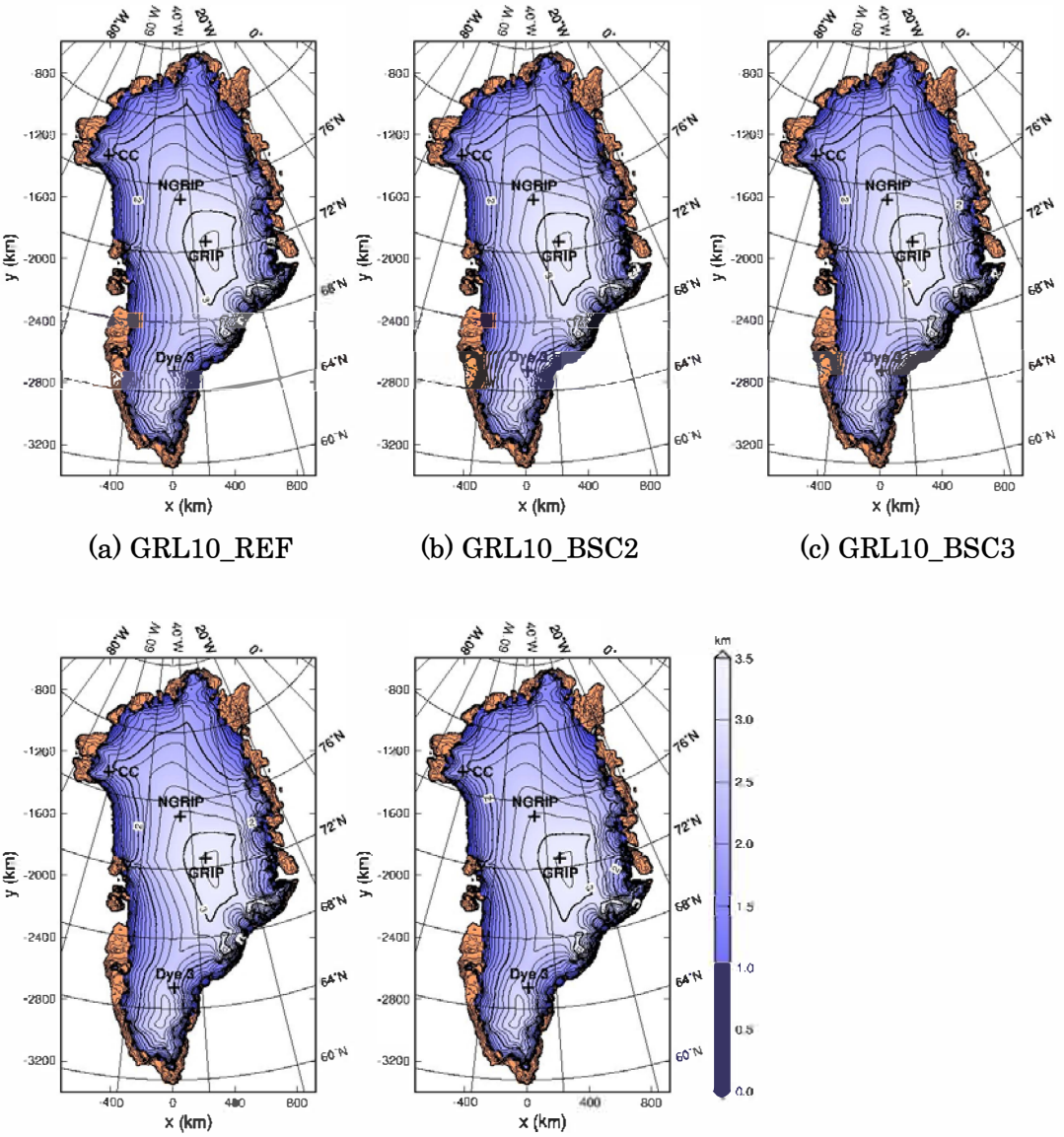

(a) GRL10_REF (b) GRL10_BSC2 (c) GRL10_BSC3

(d) GRL10_BSC4 (e) GRL10_BSC5

Figure 22. Results of surface elevation of varied basal sliding coefficient in 10-km resolution.

(a): GRL10_REF, reference simulation without the NEGIS.

(b): GRL10_BSC2, $m = 2$ at NEGIS.

(c): GRL10_BSC3, $m = 3$ at NEGIS.

(d): GRL10_BSC4, $m = 4$ at NEGIS.

(e): GRL10_BSC5, $m = 5$ at NEGIS.

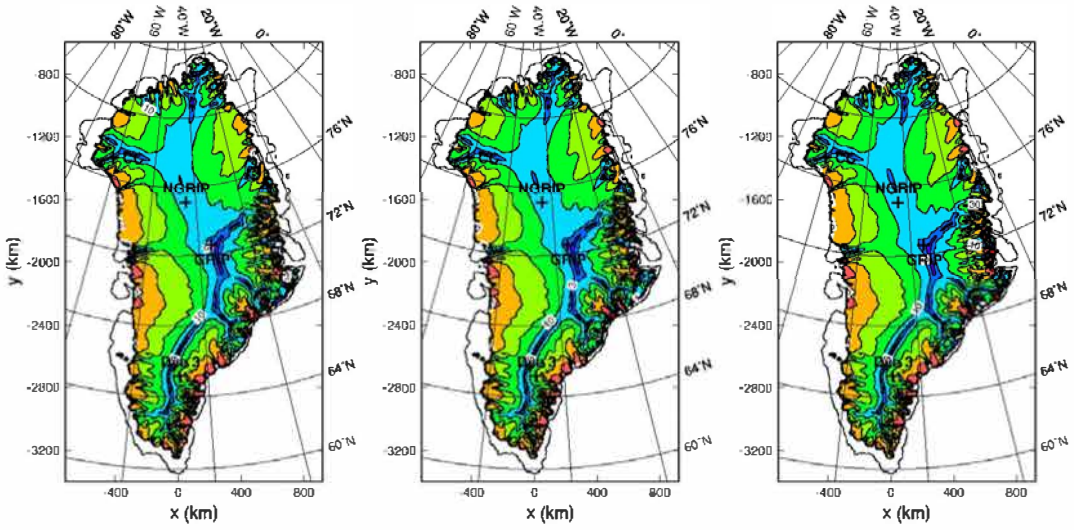

(a) GRL10_REF (b) GRL10_BSC2 (c) GRL10_BSC3

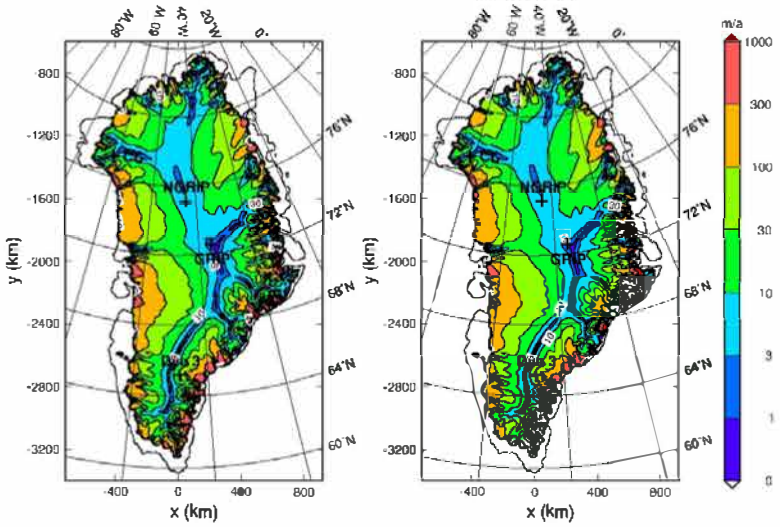

(d) GRL10_BSC4 (e) GRL10_BSC5

Figure 23. Results of surface velocity of varied basal sliding coefficient in 10-km resolution.

(a): GRL10_REF, reference simulation without the NEGIS.

(b): GRL10_BSC2, $m = 2$ at NEGIS.

(c): GRL10_BSC3, $m = 3$ at NEGIS.

(d): GRL10_BSC4, $m = 4$ at NEGIS.

(e): GRL10_BSC5, $m = 5$ at NEGIS.

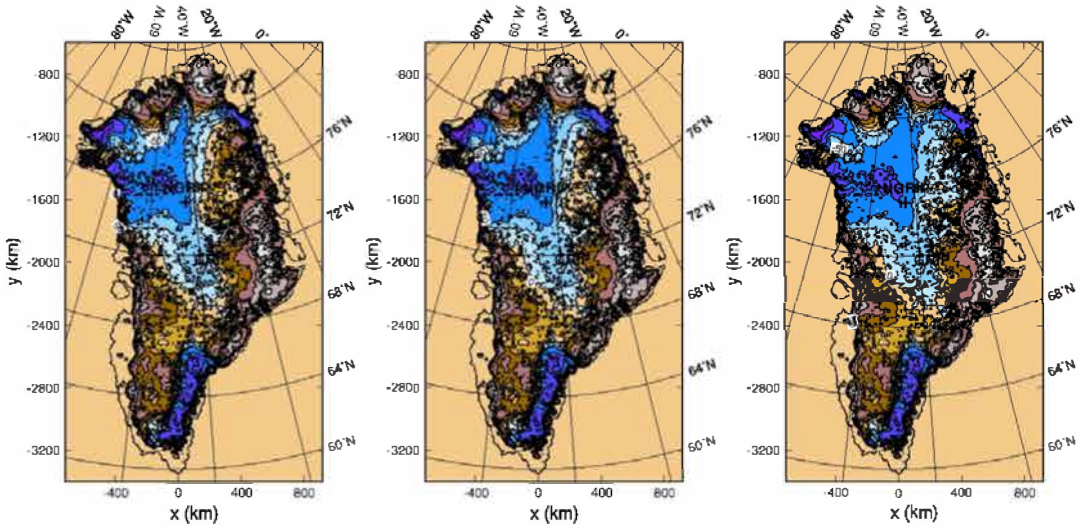

(a) GRL10_REF (b) GRL10_BSC2 (c) GRL10_BSC3

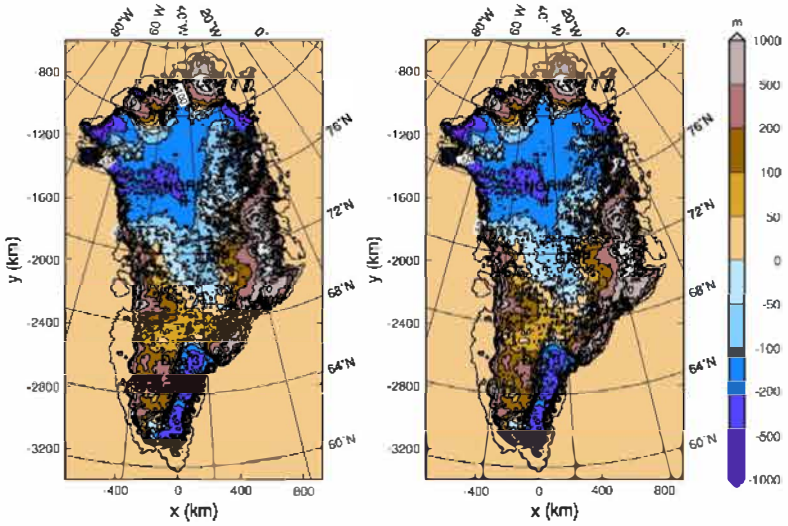

(d) GRL10_BSC4 (e) GRL10_BSC5

Figure 24. Results of ice-thickness deviation of varied basal sliding coefficient in 10-km resolution.

(a): GRL10_REF, reference simulation without the NEGIS.

(b): GRL10_BSC2, $m = 2$ at NEGIS.

(c): GRL10_BSC3, $m = 3$ at NEGIS.

(d): GRL10_BSC4, $m = 4$ at NEGIS.

(e): GRL10_BSC5, $m = 5$ at NEGIS.

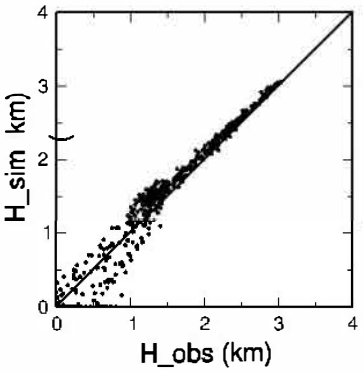

(a) GRL10_REF

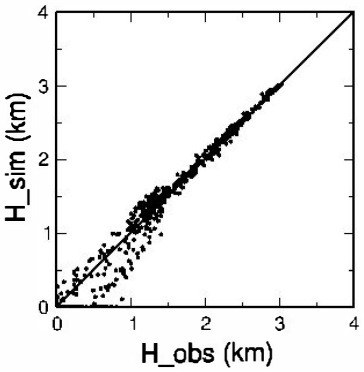

(b) GRL10_BSC2

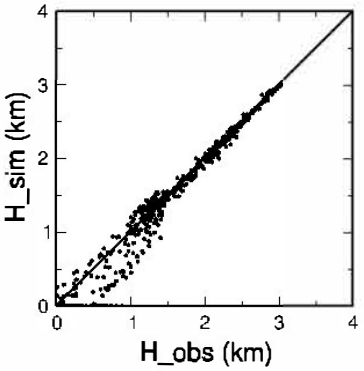

(c) GRL10_BSC3

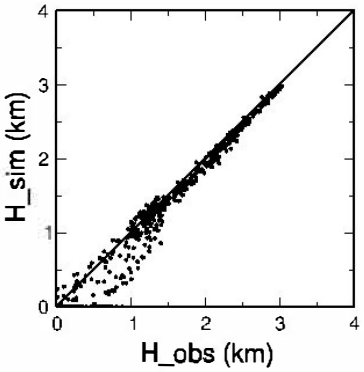

(d) GRL10_BSC4

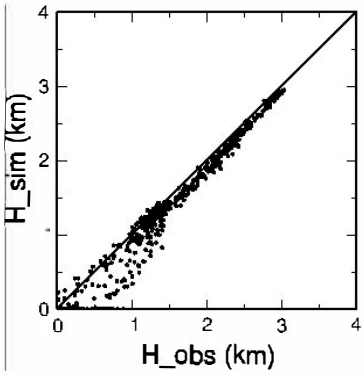

(e) GRL10_BSC5

Figure 25. Scatter plots of ice thickness of GRL10_REF and GRL10_BSC, varied basal sliding coefficient in 10-km resolution.

(a): GRL10_REF, reference simulation without the NEGIS.

(b): GRL10_BSC2, $m = 2$ at NEGIS.

(c): GRL10_BSC3, $m = 3$ at NEGIS.

(d): GRL10_BSC4, $m = 4$ at NEGIS.

(e): GRL10_BSC5, $m = 5$ at NEGIS.

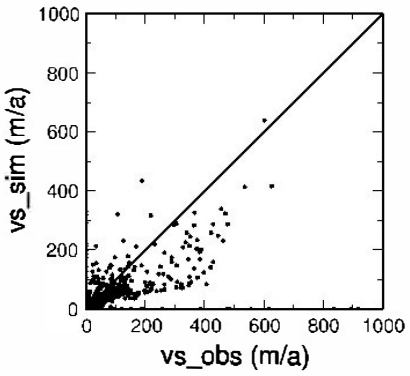

(a) GRL10_REF

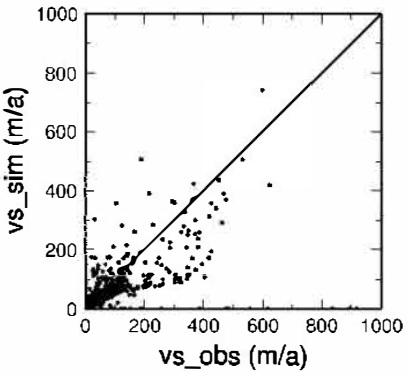

(b) GRL10_BSC2

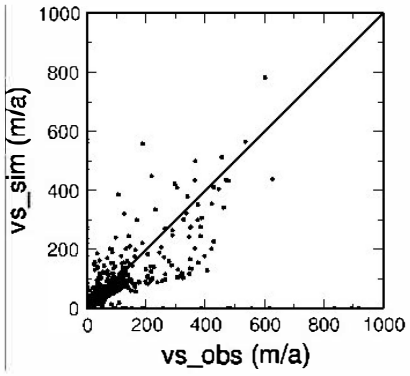

(c) GRL10_BSC3

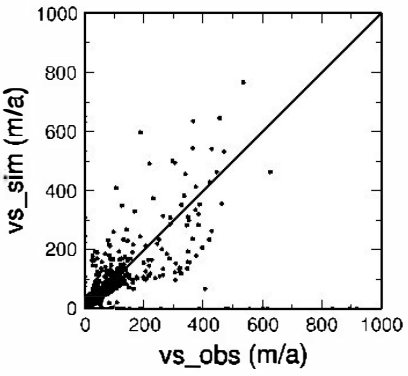

(d) GRL10_BSC4

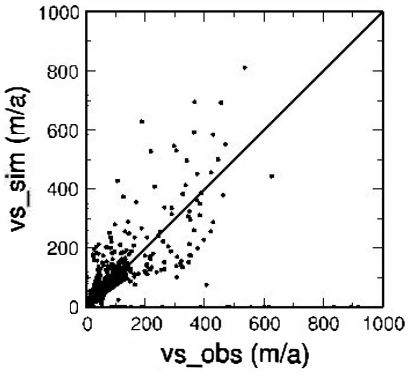

(e) GRL10_BSC5

Figure 26. Scatter plots surface velocity of GRL10_REF and GRL10_BSC, varied basal sliding coefficient in 10-km resolution.

(a): GRL10_REF, reference simulation without the NEGIS.

(b): GRL10_BSC2, $m = 2$ at NEGIS.

(c): GRL10_BSC3, $m = 3$ at NEGIS.

(d): GRL10_BSC4, $m = 4$ at NEGIS.

(e): GRL10_BSC5, $m = 5$ at NEGIS.

4.2.3 Results and discussion of simulations with varied basal sliding coefficient for linear basal sliding (GRL10_ BSCL)

Although it is probably not realistic since the bed underlying ice is hardrock in Greenland, as a comparison to GRL10_BSC the stress and pressure exponents in the sliding law are now chosen as $p = 1, q = 0$ only for the NEGIS area. This setting is usually used for soft and deformable sediment (e.g. Greve et al. 2006). In these simulations, the basal sliding coefficients C_b are set to fit the linear flow, and are chosen as 1.0 x 10^{-3} m / a Pa (GRL10_BSCL2), 1.5 x 10^{-3} m / a Pa (GRL10_BSCL3), 1.75 x 10^{-3} m / a Pa (GRL10_BSCL4), 2.0 x 10^{-3} m / a Pa (GRL10_BSCL5), 1.0 x 10^{-2} m / a Pa (GRL10_BSCL6).

Results are shown in Figure 27(a) ~ (c) for the surface elevation, surface velocity and deviation of ice thickness, respectively. The scatter plots of ice thickness and surface velocity are shown in Figure 27(d) and (e). The results for the ice thickness show that the minimum of 'mean of misfit' is - 1.329 m in GRL10_BSCL5 (C_b = 2.0 x 10^{-3} m / a Pa), and the minimum of 'RMS of misfit' is 180.4 m in GRL10_BSCL4 (C_b = 1.75 x 10^{-3} m / a Pa). On the other hand, for the surface velocity of ice, the minimum of 'mean of misfit' is + 0.5204 m / a in GRL10_BSCL3 (C_b = 1.5 x 10^{-3} m / a Pa), and the minimum of 'RMS of misfit' is 70.64 m / a in GRL10_BSCL4. These results lead to the conclusion that the most plausible value of C_b is 1.75 x 10^{-3} m / a Pa. However, in the scatter plots of ice thickness in GRL10_BSCL4 (Figure 27(d)), the points are not positioned well on the minimum-deviation line, and it shows lower results in the areas of thin ice and higher results in the areas of thicker ice. Non-linear sliding gives clearly better results, and, consequently, we discard linear in favor of non-linear sliding.

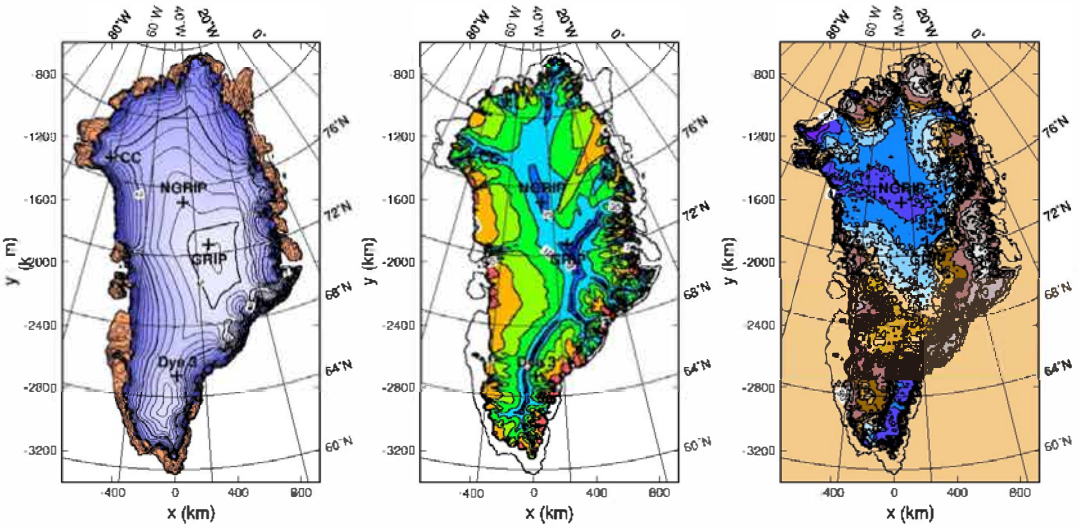

(a) GRL10_BSCL4 (b) GRL10_BSCL4 (c) GRL10_BSCL4

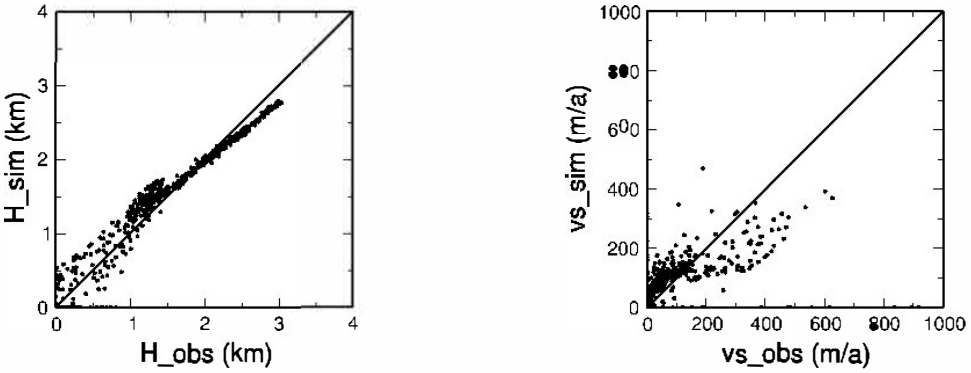

(d) GRL10_BSCL4 (e) GRL10_BSCL4

Figure 27. Results of basal sliding coefficient of the linear basal sliding law.
C_b is 1.75 x 10^{-3} m / a Pa (best value in linear laws); GRL10_BSCL4
(a): GRL10_BSCL4 surface elevation.
(b): GRL10_BSCL4 surface velocity.
(c): GRL10_BSCL4 deviation of ice thickness.
(d): GRL10_BSCL4 scatter plots of ice thickness.
(e): GRL10_BSCL4 scatter plots of surface velocity

4.2.4 Conclusion of GRL10

In the paleoclimatic simulations of GRL10, I get the most suitable value of $\widetilde{C}_b$ as 3 times normal basal sliding (sliding enhancement factor $m = 3$), in the simulations with varied basal sliding coefficient for the non-linear sliding law, while for the linear sliding law, the most suitable value is C_b = 1.75 x 10^{-3} m / a Pa. Comparison of the minima of mean and RMS misfits of the ice thickness and the surface velocity shows that the non-linear sliding law is clearly favorable, and we conclude that the NEGIS is best represented by non-linear sliding ($p = 3, q = 2$) with a sliding enhancement factor $m = 3$.

Table 2. Misfits for the non-liner basal sliding law (GRL10_BSC simulations)

Thickness of ice	REF $\widetilde{C}_b = 11.2$ m / a Pa $m = 1$	BSC2 $\widetilde{C}_b = 22.4$ m / a Pa $m = 2$	BSC3 $\widetilde{C}_b = 33.6$ m / a Pa $m = 3$	BSC4 $\widetilde{C}_b = 44.8$ m / a Pa $m = 4$	BSC5 $\widetilde{C}_b = 56.0$ m / a Pa $m = 5$
Mean of misfit	+ 75.33 m	+ 12.20 m	- 37.80 m	- 80.63 m	- 116.6 m
RMS of misfit	162.9 m	139.2 m	137.1 m	153.2 m	173.5 m

Surface velocity of ice	REF $\widetilde{C}_b = 11.2$ m / a Pa $m = 1$	BSC2 $\widetilde{C}_b = 22.4$ m / a Pa $m = 2$	BSC3 $\widetilde{C}_b = 33.6$ m / a Pa $m = 3$	BSC4 $\widetilde{C}_b = 44.8$ m / a Pa $m = 4$	BSC5 $\widetilde{C}_b = 56.0$ m / a Pa $m = 5$
Mean of misfit	- 38.54 m / a	- 24.74 m / a	- 13.05 m / a	- 0.883 m / a	+ 9.35 m / a
RMS of misfit	78.68 m / a	71.23 m / a	66.52 m / a	68.72 m / a	72.32 m / a

Table 3. Misfits for the linear basal sliding law (GRL10_BSCL simulations)

Thickness of ice	REF $\widetilde{C}_b = 11.2$ m / a Pa	BSCL2 $C_b =$ 1.0×10^{-3} m / a Pa	BSCL3 $C_b =$ 1.5×10^{-3} m / a Pa	BSCL4 $C_b =$ 1.75×10^{-3} m / a Pa	BSCL5 $C_b =$ 2.0×10^{-3} m / a Pa	BSCL6 $C_b =$ 1.0×10^{-2} m / a Pa
Mean of misfit	+ 75.33 m	+ 99.56 m	+ 48.42 m	+ 23.73 m	- 1.329 m	- 421.9 m
RMS of misfit	162.9 m	190.1 m	180.4 m	180.4 m	186.1 m	524.8 m

Surface velocity of ice	REF $\widetilde{C}_b = 11.2$ m / a Pa	BSCL2 $C_b =$ 1.0×10^{-3} m / a Pa	BSCL3 $C_b =$ 1.5×10^{-3} m / a Pa	BSCL4 $C_b =$ 1.75×10^{-3} m / a Pa	BSCL5 $C_b =$ 2.0×10^{-3} m / a Pa	BSCL6 $C_b =$ 1.0×10^{-2} m / a Pa
Mean of misfit	+ 75.33 m / a	- 18.36 m / a	+ 0.5204 m / a	+ 9.973 m / a	+ 18.86 m / a	+ 213.0 m / a
RMS of misfit	162.9 m / a	76.43 m / a	71.00 m / a	70.64 m / a	71.37 m / a	228.2 m / a

5 Future simulations

5.1 Set-up of WRE10

The effect of global warming on ice sheets is a remarkable subject, and a lot of researches rrelevant to the topic have been reported (e.g. in the third assessment report of IPCC, in Climate Change 2001: Impacts, Adaptation and Vulnerability) recently. To consider the warming climatic effect on the Greenland ice sheet, I carry out future simulations under global warming scenarios. In these runs, horizontal resolution is 10 km, which leads to 164 by 280 grid points. The domains of the entire ice sheet and the NEGIS are the same as in the GRL10 runs. Climatic forcing of global warming simulations is taken from the WRE scenarios which I mentioned in Section 3.2.3. Model time for the simulations is from 1990 AD to 2350 AD, and the time step for all model components is 1 a.

5.2 Results and discussion of the reference simulation without surface meltwater effect and without NEGIS (WRE10_WRE_REF)

In the reference simulations, the paleoclimatic reference run GRL10_REF without NEGIS effects (basal sliding coefficient, surface meltwater coefficient) is used as initial condition. The reference runs are carried out under WRE scenarios, WRE450, WRE550, WRE650, WRE750, WRE1000, and are named as WRE10_WRE450_REF, WRE10_WRE550_REF, WRE10_WRE650_REF, WRE10_WRE750_REF, WRE10_WRE1000_REF, respectively.

Figures 28(a) and 28(c) are the surface-elevation results of WRE10_WRE450_REF and WRE10_WRE1000_REF. Surface elevations of the ice sheet lowers significantly on the entire ice sheet in WRE10_WRE1000_REF compared to WRE10_WRE450_REF. Ice-covered areas also diminished in WRE10_WRE1000_REF everywhere in the ice sheet, but it is more evident in the south-west part of the ice sheet.

The effect of climate warming is already clear here without NEGIS and surface meltwater effects. It demonstrates that the temperature rise due to global warming affects the ice sheet strongly by surface melting.

5.3 Results and discussion of simulations with enhanced basal sliding and surface meltwater effect for the NEGIS (WRE10_WRE_SMW)

The best result of GRL10_BSC3 (sliding enhancement factor $m = 3$) in the paleoclimatic simulations is used as the initial condition for the experiments in this section. Here I implemented both the basal sliding effect and the surface meltwater effect with the coefficient $\widetilde{C}_{b,smw}$ defined in Equation (3.11). The surface meltwater coefficient γ is set like for the GRL20_SMW runs as 0.1 a / m (WRE10_WRE_SMW0.1), 0 a / m (WRE10_WRE_SMW0), 1 a / m (WRE10_WRE_SMW1), 2 a / m (WRE10_WRE_SMW2), 3 a / m WRE10_WRE_SMW3), 4 a / m (WRE10_WRE_SMW4), 5 a / m (WRE10_WRE_SMW5), 6 a / m (WRE10_WRE_SMW6). The climate forcing is the same as for the WRE reference runs. Five scenarios for climate forcing and six conditions for the surface meltwater coefficient (γ = 0 ~ 6 a / m) produce 30 different simulations.

Figures 28(b), 28(c), 28(e), and 28(f) are the results of surface elevations for WRE10_WRE450_SMW0.1, WRE10_WRE450_SMW6, WRE10_WRE1000_SMW0.1 and WRE10_WRE450_SMW6, respectively. Figure 29(a) is the time series of the total ice volume for the different WRE scenarios, and Figure 29(b) is the time series of the total ice volume for different values of γ and the reference run. Similarly Figure 29(a) and (b), 30(a) shows the time series of freshwater discharge for the different WRE scenarios, and 30(b) shows the time series of freshwater discharge for different values of γ and the reference run, respectively. The use of different values for γ results in small differences over the WRE scenarios. The runs with γ = 0.1 a / m, which was estimated by observational data, do not show any visible difference from the reference run for both WRE450 and WRE1000. Even in the case of the most extreme value of 6 a / m, its effects on the ice volume and water discharge are quite small, and the results are nearly the same as the reference simulations. The ice sheet decay due to the meltwater effect is limited to the north-east area of the ice sheet, and does not spread outward of the ice stream. On the other hand, the influence of the different climate scenarios on the results is much larger than that of the surface meltwater. It is very clear that the variation of WRE scenarios affects the ice volume strongly and diminishes the ice sheet.

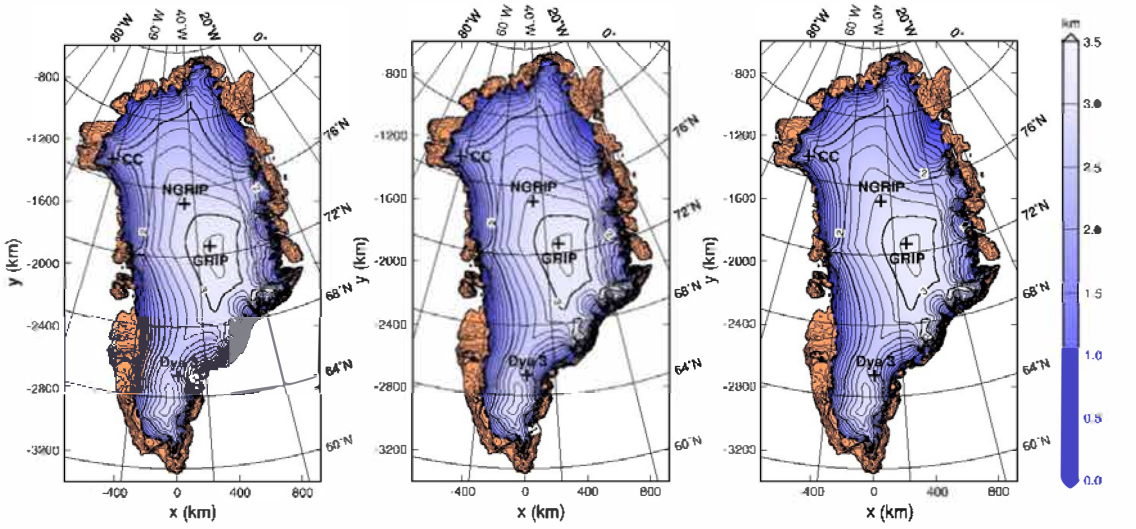

(a) WRE450_REF (b) WRE450_SMW0.1 (c) WRE450_SMW6

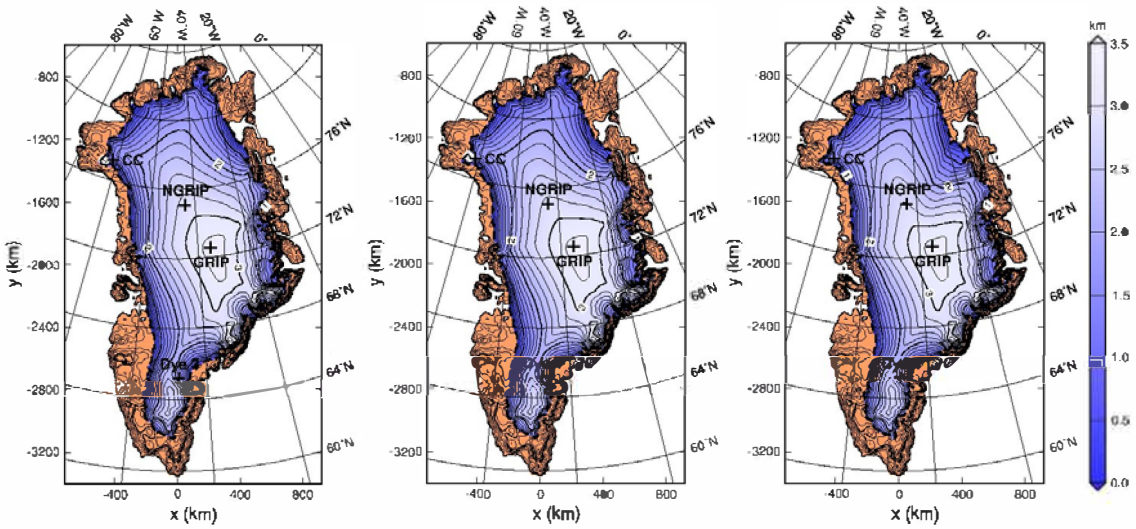

(d) WRE1000_REF (e) WRE1000_SMW0.1 (f) WRE1000_SMW6

Figure 28. Results of surface elevation of varied surface meltwater coefficient and the sliding enhancement factor $m = 3$ at NEGIS in 10-km resolution under WRE scenarios.

(a): WRE450_REF, no NEGIS effect by basal sliding coefficient, and γ = 0 a / m at NEGIS.

(b): WRE450_SMW0.1, γ = 0.1 a / m at NEGIS.

(c): WRE450_SMW6, γ = 6 a / m NEGIS.

(d): WRE1000_REF, no NEGIS effect by basal sliding coefficient, and γ = 0 a / m at NEGIS.

(e): WRE1000_SMW0.1, γ = 0.1 a / m at NEGIS.

(f): WRE1000_SMW6, γ = 6 a / m at NEGIS.

(a)

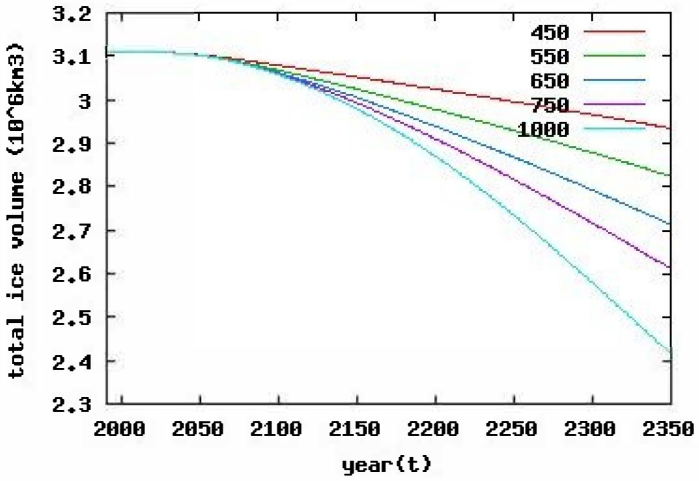

(b)

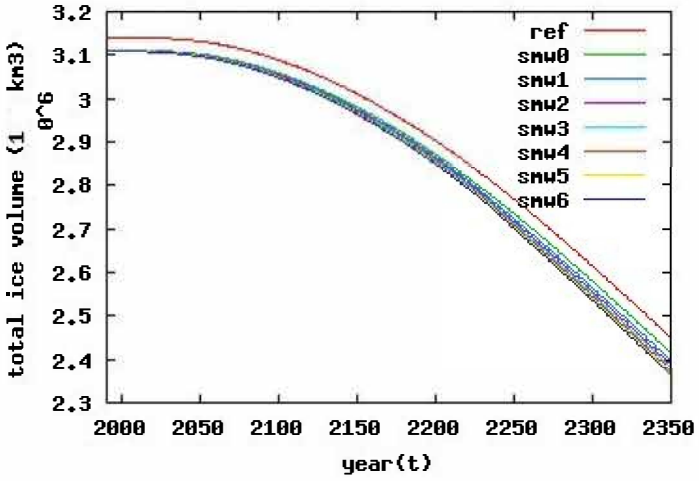

Figure 29(a): Time series of total ice volume with variation of WRE scenarios, surface meltwater coefficient γ = 0 a / m (SMW0).

Figure 29(b): Time series of total ice volume with variation of surface meltwater coefficient γ from 0 to 6 a / m under the WRE1000 scenario.

(a)

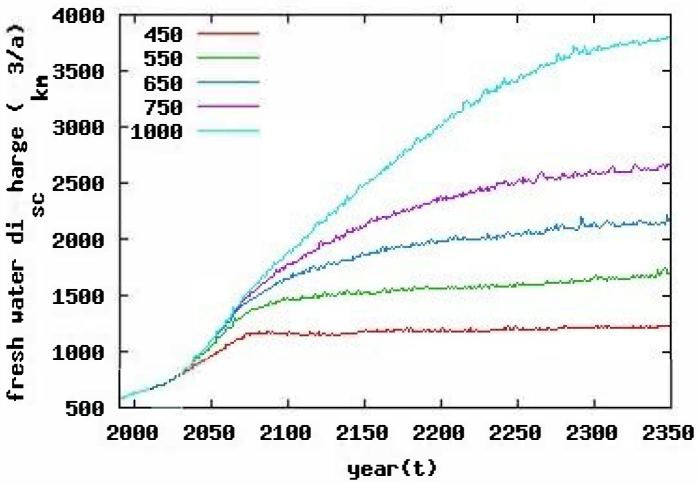

(b)

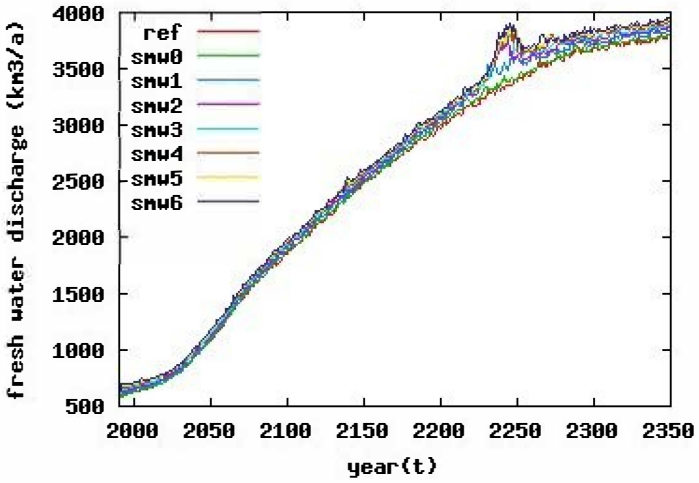

Figure 30(a): Time series of freshwater discharge with variation of WRE scenarios, surface meltwater coefficient γ = 0 a / m (SMW0).

Figure 30(b): Time series of freshwater discharge with variation of surface meltwater coefficient γ from 0 to 6 a / m under the WRE1000 scenario.

5.3' Mini surge

In addition to the results, an interesting feature can be seen in the time series of freshwater discharge in Figure 30(b). Some peaks around 2250 AD appear in most of the experiments with a surface meltwater coefficient of 1 to 6 a / m under the warming scenarios. Although it is too little amount to affect the total ice volume, it is a significant event in almost every simulation with surface meltwater effects. I assume that these peaks are mini surges which are caused by saturated surface meltwater penetrating down into the interior ice in the NEGIS area.

A surge is an event in which a part of glacier or ice sheet flows at a much faster speed than normal over a short period. Surges have been observed in glaciers and ice sheets at different locations; however, their periodic mechanisms of a few decadal cycles are still unknown (Naruse 1990). A prominent phenomenon was first observed in Variegated Glacier from 1982 to 1983, that indicates the relation between glacial basal conditions and surges (Kamb et al. 1985). They concluded that, when the water pressure at the base increases, it accelerates basal sliding of ice flow markedly, and then the acceleration causes the surge.

In order to analyze these mini surges, detailed simulations are carried out in shorter periods of Figure 30(b) during the surges. The simulations are used the same data as shown in Figure 30(b), GRL10_SMW. From the time series of freshwater discharge in each scenario, I re-plot the output of the time series while focusing on the appearance of the surges.

Figures 31(a) ~ (e) are the results of 'mini surge' outputs under the WRE450, WRE550, WRE650, WRE750 and WRE1000 scenarios, respectively. The onset of the mini surges varies within a few decades, which start in ~ 2230 AD in WRE1000, 2250 AD in WRE750, 2270 AD in WRE650, 2320 AD in WRE550, whereas there is no appearance by the end of the runs (2350 AD) in WRE450. The range of the freshwater discharge during the surges is about 500 km^3 / a in all scenarios except for WRE450 with no mini surge appearance.

As for the reason of the shift of onset of the surges, it can be presumed that the total amount of the water in the ice at the margin is related to the air temperature. The meltwater (at the surface, the base and the interior of the ice) saturates the ice in warmer areas at the ice sheet, usually at margins and lower areas. It is assumed that the amount of water is proportional to the atmospheric temperature, that is, it corresponds to the WRE scenarios.

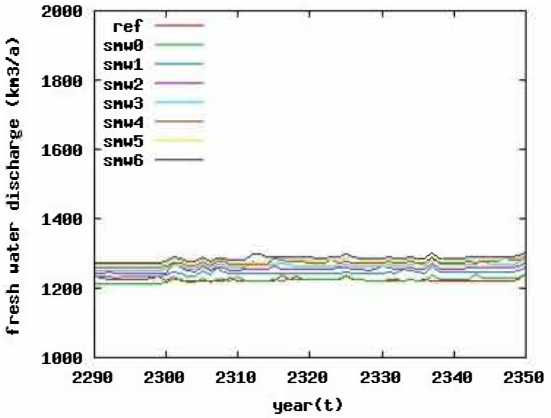

(a) WRE450

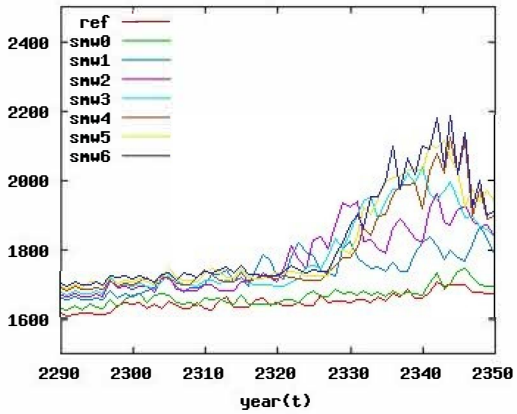

(b) WRE550

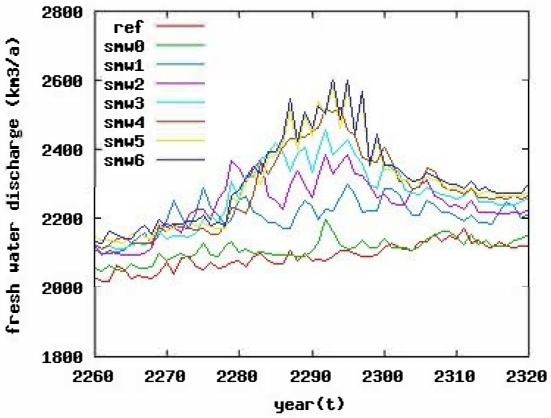

(c) WRE650

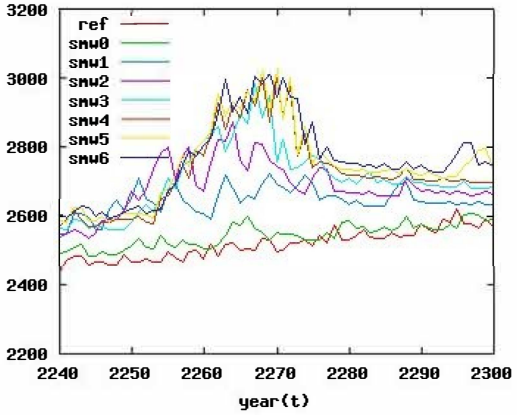

(d) WRE750

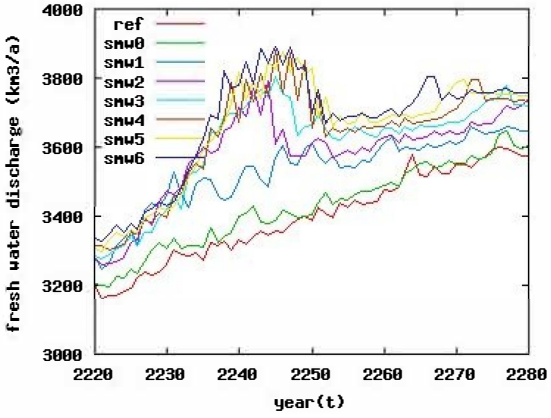

(c) WRE1000

Figure 31.

Detailed output of mini-surges in freshwater discharge with variation of the surface meltwater coefficient γ from 0 to 6 a / m.

(a): WRE450 scenario.

(b): WRE550 scenario.

(c): WRE650 scenario.

(d): WRE750 scenario.

(e): WRE1000 scenario.

5.4 Results and discussion of simulations with enhanced basal sliding for the NEGIS and surface meltwater effect for the entire ice sheet (WRE10_WRE_SMWALL)

As a further series of experiments, I impose the surface meltwater effect on the entire Greenland ice sheet, instead of limiting it to the NEGIS area. The modified basal sliding law (3.12) is used for the whole domain, and the WRE 450 and WRE1000 scenarios are run with surface meltwater coefficients of γ = 0.1 a / m, 1 a / m, and 6 a / m (WRE10_WRE450_SMWALL0.1, WRE10_WRE1000_SMWALL0.1, WRE10_WRE450_SMWALL1, WRE10_WRE1000_SMWALL1, WRE10_WRE450_SMWALL6, and WRE10_WRE1000_SMWALL6), respectively.

Figures 32(a) ~ 32(f) show the surface-elevation results of these simulations. In the WRE1000 runs, the increase of γ affects the ice volume reduction stronger than in the WRE450 runs. In addition, the effects of surface meltwater are quite large and significant especially in the southern part of the Greenland ice sheet such that the ice-sheet decay is enormous.

The difference of the effect of γ in the warming scenarios suggests that the surface meltwater effect on ice is stronger when climate conditions get warmer. The large ice shrinking in the southern part of Greenland can be explained by the setting of the degree-day factors β for ice melt and snow melt (Tarasov and Peltier 2002), even though the horizontally uniform precipitation and temperature changes are given on the whole Greenland ice sheet, and the basal topography is higher in the southern part of Greenland. In reality, the temperatures are generally higher in the south, so that ice melt is much more sensitive to the global warming.

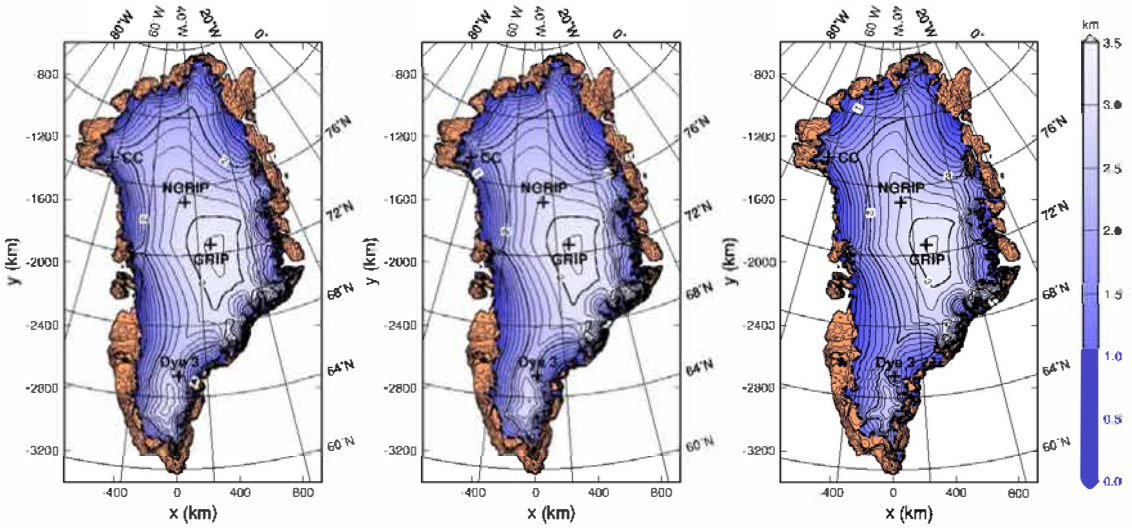

(a) WRE450_SMWALL0.1 (b) WRE450_SMWALL1 (c) WRE450_SMWALL6

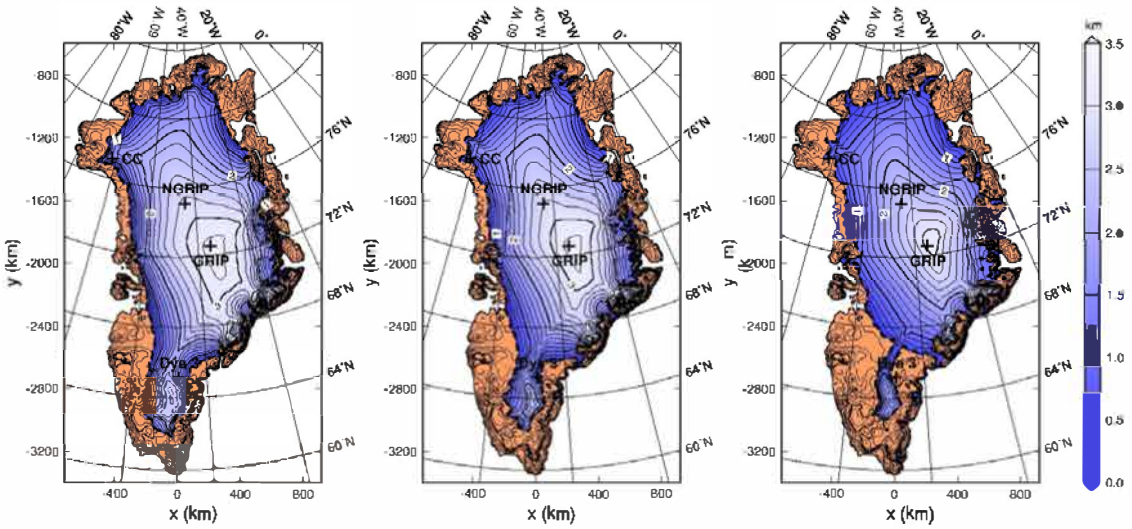

(d) WRE1000_SMWALL0.1 (e) WRE1000_SMWALL1 (f) WRE1000_SMWALL6

Figure 32. Results of surface elevation of varied surface meltwater coefficient on the entire Greenland ice sheet and the sliding enhancement factor $m = 3$ at NEGIS in 10-km resolution under WRE scenarios.

(a): WRE450_SMWALL0.1, γ = 0.1 a / m.

(b): WRE450_SMWALL1, γ = 1 a / m.

(c): WRE450_SMWALL6, γ = 6 a / m.

(d): WRE1000_SMWALL0.1, γ = 0.1 a / m.

(e): WRE1000_SMWALL1, γ = 1 a / m.

(f): WRE1000_SMWALL6, γ = 6 a / m.

5.5 Conclusion of WRE10

In the results of WRE10, it is revealed that the climate scenarios, that is, the increases of atmospheric temperature, change the simulation results significantly. WRE scenarios still assume the stabilization of CO_2 in the atmosphere, nevertheless the concentration of CO_2 today is increasing without any sign of stabilization (e.g. IPCC, Third Assessment Report, Climate Change 2001: The Scientific Basis). It indicates that further melting can be expected with the increase of the greenhouse-gas effect on the earth.

Surface meltwater at the NEGIS shows only a small effect on the ice sheet volume. Different values of the surface meltwater coefficient γ change the total ice volume slightly, and cause a small acceleration of ice sheet decay, but the melted areas are limited in north-east Greenland. Regarding freshwater discharge, the results are essentially the same as those of the total ice volume, that is to say, the effects of the variation of global warming scenarios are much stronger than the effects of the variation of the surface meltwater coefficient. The curious feature of mini-surges is found with surface meltwater effects in almost all WRE scenarios. This phenomenon will probably explain the important role of surface meltwater in the dynamics of ice sheet under warming climates.

By contrast, the experiments with a surface meltwater effect on the entire ice sheet show a strong impact on the future volume change of the ice sheet for surface meltwater coefficients which are at least an order of magnitude larger than an estimate for one site in central west Greenland (Section 3.2.4). It is significant especially in the southern part, suggesting that the generally warmer climate (higher temperature) in that region plays a key role. I would suggest that, if the surface temperature of the ice sheet rises as it is expected from the ongoing global warming, the saturated melt water in ice increases as the increase of accumulation areas, and its contribution to the acceleration of ice flow will be no more negligible.

6. Summary

The Greenland ice sheet was simulated with the ice-sheet model SICOPOLIS, and two observational features, the NEGIS and the surface meltwater effect, were implemented. The NEGIS was modeled by introducing a constant sliding enhancement factor $m > 1$ in the observed area of the fast ice flow, while the surface meltwater effect was included by further enhancing basal sliding proportional to the meltwater rate M with the surface meltwater coefficient γ.

In the paleoclimatic simulations, we succeeded in the reconstruction of the NEGIS by tuning the basal sliding coefficient. From the results of the paleoclimatic simulations of GRL10 and GRL20, we conclude that the best value for the sliding enhancement factor is $m = 3$, that is , basal sliding in the NEGIS area is three times stronger than normal basal sliding (while preserving the non-linear, hard-rock type of sliding). The effect of surface meltwater on ice volume reductions in paleoclimatic runs are small and limited to near the margins where it is enough warm to produce meltwater.

Then, we tried to investigate the effect of surface meltwater in the future simulations WRE10 under global warming conditions. The effect of the surface meltwater on basal sliding, which is applied only at the NEGIS, gives only a small influence on the ice sheet, and the influence is limited to the northeast area. Nevertheless, climate conditions which are introduced as WRE scenarios of global warming affects the future evolution of the ice sheet significantly. Further, when the effect of the surface meltwater is implemented to the entire ice sheet, its impact on ice decay seems drastic, but only if I use a value for the coefficient much larger than a local estimate from data.

As an unforeseen event in the future simulations, the existence of peaks in the freshwater discharge, which seemed like mini-surges, was identified. They appeared only when the surface meltwater effect was included. Nevertheless, the corresponding water discharges of the events were small compared to the total volume of the Greenland ice sheet. The underlying physical conditions, such as basal friction and basal temperatures during the surges, need to be clarified in future studies.

7. Acknowledgments

The author has achieved to work on the earth environmental science. I could encounter the most splendid scientific field for me, glaciology in the Institute of Low Temperature Science. Snow and ice had attracted me without any reason, and glaciers fascinated me as well.

I am obliged to Professor Ralf Greve for all the support in accomplishment of my master thesis. His instruction and advice in the thesis and his thoughtful suggestions had led me the achievement of my study in Hokkaido University. I would like to also thank him for teaching the very interesting and beneficial lecture of dynamics of ice sheets and glaciers, lecture of international communication, and initiated the knowledge of Fortran programs through SICOPOLIS.

Professor Takeo Hondoh is appreciated for his invaluable suggestions, Associate Professor Takayuki Shiraiwa for his considerable comments. I am grateful to Dr. Shin Sugiyama for his delicate advice and teaching for my study and his lecture. Dr. Tetsuo Sueyoshi greatly helped me in my working of the thesis, and Dr. Hakime Seddik showed the programming skills for me. All students and staffs of Experimental and Theoretical Glaciology Group are appreciated for supporting my study and my life in Sapporo.

The author wished to thank Professor Ian Joughin in University of Washington for kindly sending the data set providing the complete mapping of the Northeast Greenland Ice Stream, and Ms Weili Wang in NASA Goddard Space Flight Center for the transparencies of her work about 'Modeling investigation of ice sheet flow enhanced by the surface melt-induced basal sliding' presented in IGS meeting in 2005. Finally, I express my appreciation to Dr. Fuyuki Saito and Dr. Abe-Ouchi Ayako in CCSR for their encouragements to my work.

8. References

Bamber, J. L., S. Ekholm and W. B. Krabill. 2001a. A new, high-resolution digital elevation model of Greenland fully validated with airborne laser altimeter data. *J. Geophys. Res.*, 106(B4), 6733-6745.

Bamber, J. L., R. L. Layberry and S. P. Gogenini. 2001b. A new ice thickness and bedrock dataset for the Greenland ice sheet 1. Measurement, data reduction, and errors. *J. Geophys. Res.*, 106(D24), 33773-33780.

Bamber, J. L., R. L. Layberry and S. P. Gogenini. 2001c. A new ice thickness and bedrock dataset for the Greenland ice sheet 2. Relationship between dynamics and basal topography. *J. Geophys. Res.*, 106(D24), 33781-33788.

Braithwaite, R. J. and O. B. Olesen. 1989. Calculation of glacier ablation from air temperature, West Greenland. *In Oerlemans, J., ed. Glacier fluctuations and climatic change.* Dordrecht, etc., Kluwer Academic Publishers, 219-233.

Calanca, P., H. Gilgen, S. Ekholm and A. Ohmura. 2000. Gridded temperature and accumulation distributions for Greenland for use in cryospheric models. *Ann. Glaciol.*, 31, 118-120.

Calov, R. and R. Greve. 2005. A semi-analytical solution for the positive degree-day model with stochastic temperature variations. *J. Glaciol.*, 51(172), 173-175.

Calov, R. and K. Hutter. 1996. The thermomechanical response of the Greenland ice sheet to various climate scenarios. *Climate Dyn.*, 12(4), 243-260.

Chen, J. L., C. R. Wilson and B. D. Tapley. 2007. Satellite Gravity Measurements Confirm Accelerated Melting of Greenland Ice Sheet. *Science*, 313, 1958-1960.

Church, J. A., M. Gregory, P. Huybrechts, M. Kuhn, K. Lambeck, M. T. Nhuan, D. Qin and P. L. Woodworth. 2001. Changes in sea level. In: J. T. Houghton, Y. Ding, D. J. Griggs, M. Noguer, P. J. van der Linden, X. Dai, K. Maskell and C. A. Johnson (Eds.), *Climate Change 2001: The Scientific Basis. Contribution of Working Group I to the Third Assessment Report of the Intergovernmental Panel on Climate Change,* pp. 639-693. Cambridge University Press, Cambridge etc.

Cubasch, U., G. A. Meehl, G. J. Boer, R. J. Stouffer, M. Dix, A. Noda, C. A. Senior, S. Raper and K. S. Yap. 2001. Projection of future climate change. In: J. T. Houghton, Y. Ding, D. J. Griggs, M. Noguer, P. J. van der Linden, X. Dai, K. Maskell and C. A. Johnson (Eds.), *Climate Change 2001: The Scientific Basis.*

Contribution of Working Group I to the Third Assessment Report of the Intergovernmental Panel on Climate Change, pp. 525-582. Cambridge University Press, Cambridge etc.

Enting, I. G., T. M. L. Wigley and M. Heimann. 1994. Future Emissions and Concentrations of Carbon Dioxide: Key Ocean/Atmosphere/Land Analyses. *Division of Atmospheric Res.*, CSIRD, Australia.

Fahnestock, M., R. Bindschadler, R. Kwok and K. Jezek. 1993. Greenland ice sheet surface properties and ice dynamics from ERS-1 SAR imagery. *Science*, 262(5139), 1530-1534.

Fahnestock, M., W. Abdalati, I Joughin, Brozena and P. Gogineni. 2001. High geothermal heat flow, basal melt, and the origin of rapid ice flow in central Greenland. *Science*, **294** (5550), 2338-2342. doi:10.1126/science.1065370.

Forsström, P. L. and R. Greve. 2004. Simulation of the Eurasian ice sheet dynamics during the last glaciation. *Global Planet Change*, 42(1-4), 59-81. doi:10.1016/j.gloplacha.2003.11.003.

Forsström, P. L., O. Sallasmaa, R. Greve and T. Zwinger. 2003. Simulation of fast-flow features of the Fennoscandian ice sheet during the Last Glacial Maximum. *Ann. Glaciol.*, **37**, 383-389.

Greve, R. 1997a. A continuum-mechanical formulation for shallow polythermal ice sheets. *Philosophical Transactions of the Royal Society London*, **A** 355(1726), 921-974.

Greve, R. 1997b. Application of a polythermal three-dimensional ice sheet model to the Greenland ice sheet: Response to steady-state and transient climate scenarios. *J. Climate*, **10**(5), 901-918.

Greve, R. 2001. Glacial isostasy: Models for the response of the Earth to varying ice loads. In: B. Straughan, R. Greve, H. Ehrentraut and Y. Wang (Eds), *Continuum Mechanics and Applications in Geophysics and Environment*, pp. 307-325. Springer, Berlin etc.

Greve, R. 2004. Evolution and dynamics of the Greenland ice sheet over past glacial-interglacial cycles and in future climate-warming scenarios. *Proceedings of the 5th international workshop on global change: Connection to the Arctic (GCCA5)* 42-45.

Greve, R. 2005a. Relation of measured basal temperatures and the spatial distribution of the geothermal heat flux for the Greenland ice sheet. *Ann. Glaciol.*, **42**, 424-432.

Greve, R. 2005b. *Dynamics of ice sheets and glaciers.*

Lecture notes Hokkaido University Open Course Ware, available online at http://ocw.hokudai.ac.jp/Course/GraduateSchool/EnvironmentalScienceDynamicsOfIce/.

Greve, R., and K. Hutter. 1995. Polythermal three-dimensional modeling of the Greenland ice sheet with varied geothermal heat flux. *Ann. Glaciol.*, 21, 8-12.

Greve, R., B. Mügge, D. R. Baral, O. Albrecht and A. A. Savvin. 1999. Nested high-resolution modeling of the Greenland Summit region. In: K. Hutter, Y. Wang and H. Beer (Eds), *Advances in Cold-Region Thermal Engineering and Sciences*, pp. 285-306. Springer, Berlin etc.

Greve, R., R. Takahama and R. Calov. 2006. Simulation of large-scale ice-sheet surges: The ISMIP HEINO experiments. *Polar Meteorology and Glaciology*, 20, 1-15.

Greve, R., M. Weis and K. Hutter. 1998. Paleoclimatic evolution and present conditions of the Greenland ice sheet in the vicinity of Summit: An approach by large-scale modeling. *Paleoclimates*, 2(2-3), 133-161.

Hewitt, C. D. and J. F. B. Mitchell. 1997. Radiative forcing and response of a GCM to ice age boundary conditions: cloud feed back and climate sensitivity. *Climate Dyn.*, 13(11), 821-834.

Hindmarsh, R. C. A. and E. Le Meur. 2001. Dynamical processes involved in the retreat of marine ice sheets. *J. Glaciol.*, 47(157), 271-282.

Hock, R. 2003. Temperature index melt modeling in mountain areas. *J. Hydrol.*, 282(1-2), 104-115.

Hutter, K. 1983. *Theoretical Glaciology; Material Science of Ice and the Mechanics of Glaciers and Ice Sheets.* D. Reidel Publishing Company, Dordrecht, The Netherlands.

Huybrechts, P. 2002. Sea-level change at the LGM from ice-dynamics reconstructions of the Greenland and Antarctic ice sheets during the glacial cycles. *Quaternary Sci. Rev.*, 21(1-3), 203-231.

Huybrechts, P., A. Letréguilly and N. Reeh. 1991. The Greenland ice sheet and greenhouse warming. *Palaeogeography, Palaeoclimatology, Palaeoecology (Global and Planetary Change Section)*, 89, 399-412. Elsevier Science Publishers B.V., Amsterdam.

Iken, A., H. Rothlisberger, A. Flotron and W. Haberli. 1983. *J. Glaciol.*, 29, 28.

IPCC (Intergovernmental Panel on Climate Change), Third Assessment Report, *Climate Change 2001: Impacts, The Scientific Basis*, *Adaptation and Vulnerability*.

IPCC (Intergovernmental Panel on Climate Change), Third Assessment Report, *Climate Change 2001: The Scientific Basis. Contribution of Working Group I to*

the Third Assessment Report of the Intergovernmental Panel on Climate Change, pp. 525-582. Cambridge University Press, Cambridge etc.

Joughin, I., M. Fahnestock and D. MacAyeal, J. L. Bamber, and S. P. Gogenini. 2001. Observation and analysis of ice flow in the largest Greenland ice stream. *J. Geophys. Res. Atmos.,* 106(D24). 34021-34034.

Joughin, I., W. Abdalati and M. Fahnestock. 2004. Large fluctuations on speed in Greenland's Jakovshavn Isbrae glacier. *Nature*, 432(7017), 608-610. doi:10.1038/nature03130.

Kamb W. B., C. F. Raymond, W. D. Harrison, H. Engelhardt, K. A. Echelmeyer, N. Humphrey, M. M. Brugman and T. Pfeffer. 1985. Glacier surge mechanism: 1982-1983 surge of Variegated Glacier, Alaska. *Science* 227(4686), 469-479.

Le Meur, E. and P. Huybrechts. 1996. A comparison of different ways of dealing with isostasy: examples from modeling the Antarctic ice sheet during the last glacial cycle. *Ann. Glaciol.*, 23, 309-317.

Leggett, J., W. J. Pepper, and R. J. Swart. 1992. Emissions Scenarios for the IPCC: An Update. In: *Climate Change 1992: The Supplementary Report to the IPCC Scientific Assessment* (Eds. Houghton, J.T., B. A. Callander, and S. K. Varney). Cambridge University Press, Cambridge, pp.69-95.

Letréguilly, A., N. Reeh and P. Huybrechts. 1991. The Greenland ice sheet through the last glacial-interglacial cycle. *Global Planet. Change,* 90(4), 385-394.

Marshall, S. J. and K. M. Cuffe. 2000. Peregrinations of the Greenland ice sheet divide in the last glacial cycle: implications for central Greenland ice cores. *Earth Planet. Sci. Lett.*, 179(1), 73-90.

Morland, L. W. 1984. Thermo-mechanical balances of ice sheet flows. *Geophys. Astrophys. Fuid Dyn.*, 29, 237-266

Naruse, R. 1990. *Seppyo-Jiten*. The Japanese Society of Snow and Ice Press. pp. 33.

Ohmura, A. 2004. Cryosphere During the Twentieth Century. *The State of the Planet: Frontiers and Challenges in Geophysics*. Geophysical Monograph 150, IUGG 19, 239-257. Copyright 2004 by the International Union of Geodesy and Geophysics and the American Geophysical Union. 10.1029/150GM19.

Ohmura, A., and N. Reeh. 1991. New precipitation and accumulation maps for Greenland. *J. Glacio*l., 37(125), 140-148.

Paleoclimate Modeling Intercomparison Project (PMIP, www-lsce.cea.fr/pimp).

Parizek, B. R. and R. B. Alley. 2004. Implications of increased Greenland surface melt under global-warming scenarios: ice-sheet simulations. *Quat. Sci. Rev.*, 23(9-10), 1013-1027.

Paterson, W. S. B. 1994. *The physics of glaciers*. Pergamon Press, Oxford etc., 3rd ed.

Petit, J. R., J. Jouzel, D. Raynaud, N. I. Barkov, J. M. Barnola, I. Basile, M. Bender, J. Chappellaz, M. Davis. G. Delaygue, M. Delmotte, V. M. Kotlyakov, M. Legrand, V. Y. Lipenkov, C. Lorius, L. Pepin, C. Ritz, E. Saltzman, and M. Stievenard. 1999. Climate and atmospheric history of the past 420,000 years from the Vostok ice core, Antarctica. *Nature*, **399**(6735), 429-436.

Pollack, H. N., S. J. Hurter and J. R. Johnson. 1993. Heat-flow from the Earth's interior: Analysis of the global data set. *Rev. Geophys.*, **31**(3), 267-280.

Program for Arctic Regional Climate Assessment (PARCA). Data sets from "Data and Information Service for CliC" (http://clic.npolar.no/disc/), courtesy Dr. Ian Joughin.

Reeh, N. 1991. Parameterization of melt rate and surface temperature on the Greenland ice sheet. *Polarforsch.*, **59**(3), 113-128.

Ritz, C., A. Fabré and A. Letréguilly. 1997. Sensitivity of a Greenland ice sheet model to ice flow and ablation parameters: consequences for the evolution through the last climatic cycle. *Climate Dyn.*, **13**(1), 11-24.

Saito, F., 2002. *Development of a three dimensional ice sheet model or numerical studies of Antarctic and Greenland ice sheet*. Center for Climate System Research, University of Tokyo, Japan.

Schimel, D. S. et al. 1995. Radiative Forcing of Climate Change and an Evaluation of the IPCC IS92 Emissions Scenarios (eds Houghton, J. T. et al.). *Climate Change 1994*. 35-71, Cambridge Univ. Press.

Sugiyama, S. 2005. *Support material for Advanced course in Glacier and Ice Sheet Science*. (http://wwwice.lowtem.hokudai.ac.jp/~sugishin/lecture/).

Tarasov, L. and W. R. Peltier. 2002. Greenland glacial history and local geodynamic consequences. *Geophys. J. Int.*, **150**(1), 11-24

Tarasov, L. and W. R. Peltier. 2003. Greenland glacial history, borehole constraints, and Eemian extent. *J. Geophys. Res.*, 108(B3), 2143. doi: 10.1029/2001JB001731.

Thomas, R. H., B. M. Csathó, S. Gogineni, K. C. Jezek and K. Kuivinen. 1998. Thickening of the western part of the Greenland ice sheet. *J. Glaciol,*. **44**(148), 653-658.

Weertman, J. 1957. On the sliding of glaciers. *J. Glaciol.*, **3**, 33-38.

Weidick, A., M. Kelly and O. Bennike. 2004. Late Quaternary development of the southern sector of the Greenland Ice Sheet, with particular reference to the Qassimiut lobe. *BOREAS*, **33**(4), 284-299.

Wigley T. M. L., R. Richels and J. A. Edmonds. 1996. Economic and environmental

choices in the stabilization of atmospheric CO_2 concentrations. *Letters to Nature*, **379,** 240-243.

Zwally, H. J., W. Abdalati, T. Herring, K. Larson, J. Saba and K. Steffen. 2002. Surface melt-induced acceleration of Greenland ice-sheet flow. *Science,* **297**(5579), 218-222.

van de Wal, R. S. W. 1991. Processes of buildup and retreat of the Greenland ice sheet. *J. Geophys. Res.,* **104**(D4), 3899-3906.